Relative Impacts of ENSO and Indian Ocean Dipole/Zonal Mode on Southern African Rainfall

A dissertation in fulfillment of the requirements of Masters Degree by Dissertation only in the Oceanography Department, Faculty of Science, University of Cape Town.

February 2010

By

DESMOND MANATSA

Student Number: MNTDES001

Supervisor:

Professor CHRIS REASON

Acknowledgements

Foremost I would like to express my deepest gratitude to my supervisor, Prof. Chris Reason, for his expert advice, continuous support, and valuable guidance throughout my Masters project. I particularly thank him for patiently arranging for the financial support from NRF to enable me to do this project. I am very grateful to my colleagues Dr. Matarira and Dr. Mukwada for their keen interest and support of my work. We had lots of fruitful discussions on the regional impacts of the Indian Ocean Dipole which they initially took to be very weird. I deeply appreciate their critical reading and comment that greatly assisted in shaping of an earlier version of this thesis.

Access to ENSO SST data and University of Delaware monthly rainfall data from the NCEP-NCAR reanalysis project was provided by the Climate Diagnostics Centre (CDC) at Boulder, Colorado and obtained via URL http://www.cdc.noaa.gov. JAMSTEC provided the Indian Ocean Dipole SST data through their IOD website; http://www.**jamstec**.go.jp/frsgc/. Wavelet software was provided by C. Torrance and G Compo and is available via URL: http://paos.colorado.edu/research/ wavelets/.

The following conference presentation and journal publication arising from this work is acknowledged:

1. Manatsa D, Matarira CH, Mukwada G. 2009. Relative Impacts of ENSO and Indian Ocean Dipole/zonal mode on east SADC rainfall. International Journal of Climatology. DOI: 1.1002/joc.2086.
2. Symposium 3 December 2009: Climate Variations of southern Africa and Roles of Subtropical Oceans Tokyo University, Tokyo, Japan.

I have to recognize that this thesis would have never been completed without the continuous moral support, patience and love of my wife Faith and children Kelly, Tariro and Tina. I dedicate this thesis to them.

Declaration

I know the meaning of plagiarism and declare that this thesis is to the best of my knowledge my original work except where sources have been acknowledged. I also declare that this thesis is my own unaided work, both in conception and execution, and that apart from normal guidance of my supervisor; I have received no assistance apart from those acknowledged. Except as stated below, neither the substance nor any part of the thesis has been submitted in the past, or is being, or will ever be submitted for a degree at this University, nor to any other University for the awarding of a degree. I am now presenting the thesis for examination for the Degree of Master of Science to the University of Cape Town.

DESMOND MANATSA……..	**PROFESSOR CHRIS REASON**……
Student Name	Faculty/Department Supervisor
……..	……
Signature	Signature
……..	……
Date	Date

Abstract

This thesis investigates the October to December (OND) rainfall variability over the mainland region of southeastern Africa in relation to El Niño Southern Oscillation (ENSO) and the Indian Ocean Dipole/Zonal Mode (IODZM) for the period 1950 to 1999. An empirical orthogonal function (EOF) analysis of OND rainfall field revealed that the north-south aligned areas of the eastern SADC are located in different covariability regions. This meridionally aligned dipole rainfall anomaly configuration is captured only in the dominant principal component (PC1) making it possible for the opposing rainfall anomalies of the two regions to have a common trigger. However, ENSO which has typically been invoked as the main cause for significant rainfall variability over this region cannot adequately explain this dipole rainfall anomaly pattern. The results of statistical analyses strongly indicate that positive Indian Ocean Dipole/Zonal Mode (IODZM) phase events lead to a rainfall dipole such that floods occur over the north east of the region (Tanzania) at the same time as droughts over the south east of the region (Zimbabwe, northern South Africa). On the other hand, negative IODZM phase events do not seem to lead to the reverse rainfall anomalies suggesting that the positive and negative rainfall dipoles may have rather different causes. Thus, contrary to conventional knowledge, the ENSO association to this dipole rainfall anomaly pattern is not robust but appears to be the result of the well known ENSO-IODZM connection. However, when analysed over 31-year overlapping segments, the results indicate that the sensitivity of this rainfall pattern to the IODZM is weakening from the 1990s onwards whereas that of ENSO appears to be strengthening.

TABLE OF CONTENTS

Content **Page**

LIST OF TABLES

Table **Page**

LIST OF FIGURES

Content **Page**

LIST OF APPENDICES

LIST OF ACRONYMS

Acronym	Definition
DMC	Drought Monitoring Centre
ECMWF	European Center for Medium-range Weather Forecast
ENSO	El Niño Southern Oscillation
EOF	Empirical Orthogonal Function
ESMDR	East SADC Meridional Dipole Rainfall
ESMDRI	East SADC Meridional Dipole Rainfall Index
GCM	General Circulation Model
GWS	Global Wavelet Spectra
HadISST	Hadley Centre sea ice and SST
IODZM	Indian Ocean Dipole/zonal mode
IODZMI	Indian Ocean Dipole/zonal mode Index
pIODZM	positive Indian Ocean Dipole/zonal mode
nIODZM	negative Indian Ocean Dipole/zonal mode
IRI	International Research Institute
ITCZ	Inter Tropical Convergence Zone
JFM	January to March
MAM	March to May
NAO	North Atlantic Oscillation
NCEP	US National Climate for Environmental Prediction
NESOR	Northeast SADC October to December Rainfall
NESORI	Northeast SADC October to December Rainfall Index
Niño 3.4	El Niño region 3 and 4
NOAA	Northern Ocean Atmospheric Administration
PCA	Principal Component Analysis

PC	Principal Component
SADC	Southern African Development Community
SARCOF	Southern African Regional Climate Outlook Forums
SESOR	Southeast SADC October to December Rainfall
SESORI	Southeast SADC October to December Rainfall Index
SOI	Southern Oscillation Index
SST	Sea Surface Temperature
Zim SPI	Zimbabwe Standardized Precipitation Index

CHAPTER 1:

Introduction and Literature Review

The Southern African Development Community (SADC) comprises 15 member states, with well over 220 million inhabitants. The socio economic development of this regional block, with a gross annual economic production of U$120 billion (Jury, 2002), is intrinsically and inextricably tied to rain fed agriculture. The rainfall pattern is highly variable both spatially and temporarily, and is characterized by relatively amplified frequencies of droughts and floods (e.g. Jury and Mwafulirwa 2002). Accurate seasonal to interannual climate monitoring and forecasting could significantly contribute to a reduction in extreme climate vulnerabilities. This can only be achieved through better knowledge of the regional rainfall triggering mechanisms and teleconnections.

1.1 The East SADC Rainfall and its Seasonal Forecasts

It has long been noted that the eastern SADC region (eastern part of Africa south of the equator) is characterized by an opposition in austral summer rainfall anomalies (Ropelewski and Halpert, 1989; Janowiak, 1988; Richard et al., 2001). The majority of the studies exploring this see-saw rainfall behavior on interannual time scales attributed the variations to the tropical SSTs in the western Pacific. These SST anomalies are believed to simultaneously provide a wet (dry) summer in northeast (northeast) and a dry (wet) summer in the southeastern SADC region. However, McHugh and Rogers (2001) also found this dipole like rainfall anomaly system between the two regions but surprisingly attributed the pattern to North Atlantic Oscillation (NAO).

Rainfall variability of the SADC region has also been investigated at sub regional levels. For example some authors (e.g. Nicholson and Kim, 1997; Camberlin et al., 2001; McHugh, 2006) examined the austral summer rainfall variability over the east African

region only while others investigated variability over southern Africa (Matarira, 1990; Kruger, 1999; Reason and Jagadheesha, 2005). Using observational and/or modeling studies, these authors produced extensive evidence supporting that the regional rainfall is indisputably linked to El Niño–Southern Oscillation (ENSO). Chamberlain et al. (2001) went to the extent of declaring that 'ENSO forcing is virtually undisputed in the regions bordering the Indian Ocean from equatorial Africa to South Africa'. In addition to ENSO, the SST anomaly forcing from the Atlantic Ocean and Indian Ocean has been understood to also significantly impact on east Africa (McHugh and Rogers, 2001; Mutai and Ward, 2000; McHugh, 2006) and southern Africa (Makarau and Jury, 1997; Reason and Mulenga, 1999; Rouault and Richard, 2005; Reason et al., 2006). But by assuming the process to be essentially inseparable from ENSO, these studies seem to preserve the assumed paramount role of the ENSO forcing. As a result, ENSO is considered not only as the dominant, but also as inheriting the most predictable component controlling regional rainfall (Jury et al., 2004; Nicholson, 2003).

No wonder ENSO has been adopted by the Southern African Regional Climate Outlook Forums (SARCOFs) as the primary forcing factor and predictor of the SADC seasonal rainfall since the forums inception in 1997. These SARCOFs are the products of the efforts of the International Research Institute (IRI, USA) and the WMO supported SADC Drought Monitoring Centre (DMC, Botswana) which aims at developing consensus in regional seasonal forecasts. Therefore the seasonal forecasting efforts by operational agencies and universities in the SADC region tend to rely on a combination of statistical techniques and general circulation model (GCM) outputs, which strongly depend on ENSO predictability. While the statistical rainfall forecasting schemes rely heavily on the change in the magnitude of various ENSO indices, the operational GCMs have their simulated rainfall that is more sensitive to the SSTs specified in the Pacific than to any

other external boundary forcing (Latif et al., 1999; Kumar et al., 1999). It then becomes quite apparent that the success of seasonal forecasts for the regional rainfall depends on the stationarity of the empirical relationships and the spatial consistency of ENSO impacts. However, ENSO has also been noted to fall short of accounting completely for the sub-regional rainfall variability (Goddard and Graham, 1999; Fauchereau et al., 2003; Reason and Jagadheesha, 2005; Manatsa et al., 2007, 2008).

1.2 The IODZM and its independence from ENSO

Until recently, it has been assumed that the Indian Ocean did not have an interannual ocean atmosphere coupling cycle (Merchant et al., 2006). The discovery of the Indian Ocean Dipole Zonal Mode (IODZM) as a significant coupled mode in the tropical Indian Ocean (Saji et al., 1999; Webster et al., 1999) has added a previously unknown dimension that further complicates the established regional ENSO-SADC rainfall prediction equation. The main reason is that this mode appears to have a complicated relationship with ENSO, occurring at times of ENSO extremes and at other times when the Pacific is not anomalous (Webster et al., 1999; Saji et al., 1999; Clark et al., 2003). Its complexity together with its short research history, has led some researchers like Baquero-Bernal and Latif, (2002) and Allan et al. (2001) to question its existence as well as independence from ENSO. Chambers et al. (1999) related this Indian Ocean SST dipole as an extension of the Indo-Australian node of the Southern Oscillation (SO) component of ENSO into the Indian Ocean. Thus the IODZM phenomenon had traditionally been viewed in some quarters as an artifact of the ENSO system (Black et al., 2003, Hendon, 2003; Shinoda et al., 2004). But with time, this complication has even increased in view of some authors like Wu and Kirtman (2005) who have gone to the extent of suggesting that the Indian Ocean coupling is more crucial for the atmospheric variability in the tropical Pacific rather than the reverse.

Evidence is increasingly amassing that the IODZM is a separate and distinct phenomenon (Saji and Yamagata, 2003; Ashok et al., 2004; Merchant et al., 2006). For example, some proof on the physical existence of the IODZM has been demonstrated by showing the IODZM as a physical entity which is an internal coupled mode in the Indian Ocean that at times co-occurs with ENSO extremes and occasionally, when the tropical Pacific does not display any anomalous SST behavior (Webster et al., 1999; Saji et al., 1999; Vinayachandran, 2002; Murtugudde et al., 2000; Iizuka et al., 2000, Rao et al., 2002; Yamagata et al., 2003 and Ashok et al., 2004). Annamalai and Murtugudde, (2004) noted that there is evidence on the active role played by the Indian Ocean on some of the IODZM mode events. In fact, the recent three distinctive positive IODZM events that evolved consecutively from 2006 to 2008 seem to have settled all speculation about its independence from ENSO. This rare occurrence provided ample evidence indicating that the dipole mode phenomenon is an independent atmosphere/ocean interaction in the Indian Ocean, with no causal relation to ENSO effect in the Pacific Ocean. It is however, the self sustainability of this mode and its impact on regional and global climate that is still a matter of debate (Annamalai and Murtugudde, 2004).

1.3 ENSO/IODZM and the East SADC early summer rainfall

It is important that the seasonal climate conditions over the Indian Ocean and the East SADC sector relevant to this study are briefly described. Thus setting aside the debate about the exact nature of the triggering factors of IODZM or its relationship with ENSO, we believe that there should not be a problem in appreciating that the impact of the Indian Ocean on regional climate may in fact occur through this mighty ocean atmosphere coupled mode. The SST gradients generated during the evolution of the IODZM events are quite substantial even relative to the global scale (Annamalai and

Murtugudde 2004). It is known that steep gradients of SSTs in the oceans are important in determining the specific location of precipitation over the tropics. Therefore it is highly probable that the introduction of this previously unknown anomalously strong SST gradient in the tropical Indian Ocean to the ENSO-SADC rainfall equation may alter the previously assumed facts about this particular relationship.

Moreover, this phenomenon has its peak occurrence period from September to November (Yamagata et al., 2003) coinciding primarily with the early summer rainfall of the sub region and even more importantly, is located in the most significant summer moisture source of the eastern SADC region (D'Abreton and Tyson, 1995). It is therefore only logical to expect the IODZM to have a significant influence on early summer rainfall variability over the sub region. Apparently the statistical analyses inherent in the past research, especially prior to the introduction of the IODZM mode, did not recognize the degeneracy of ENSO and IODZM. Any analysis based on the signal obtained from SST anomalies averaged over the whole tropical Indian Ocean always has a dominant ENSO signal (Ashok et al., 2004). This fact could have lead many researchers into assuming that the Indian Ocean responds passively to the Pacific phenomenon. Therefore those analyses may inherit part of the important influence of the anomalously steep tropical east-west SST gradients generated during IODZM evolution, as an apparent sole influence of ENSO on southern African rainfall. This study will attempt to show that the previous approach may have been misleading in a way.

Under normal circumstances the SSTs over the equatorial Indian Ocean are higher in the east by about 2ºC. But the occurrence of the IODZM generates anomalous cooling of SST in the southeastern equatorial Indian Ocean off Sumatra, and the anomalous warming in the western equatorial Indian Ocean. Consequently, in response to these

SST changes, the surface wind field experiences changes especially in the zonal component. Cooler waters in the eastern Indian Ocean gives rise to sustain an anomalous easterly flow along the equatorial zone. Ultimately, the atmospheric convection over the eastern (western) tropical Indian Ocean is suppressed (enhanced). This state of the Indian Ocean is identified as a positive IODZM event, which develops rapidly in boreal summer and peaks during the September to November period (Yamagata et al., 2003). The reverse situation viz. positive (negative) SST anomalies over the southeast (western) equatorial Indian Ocean and the associated intensified westerly flow are termed the negative IODZM. These opposite events generate strong zonal SST gradients which are considered to be the most important climatic phenomena to occur in the tropical Indian Ocean (Hastenrath et al., 2002). Figure 1 summarizes these processes. In fact these climatic features have been extensively described and illustrated in several papers (e.g. Saji et al., 1999; Webster et al., 1999; Black et al., 2003; Saji and Yamagata, 2003; Ashok et al., 2004)

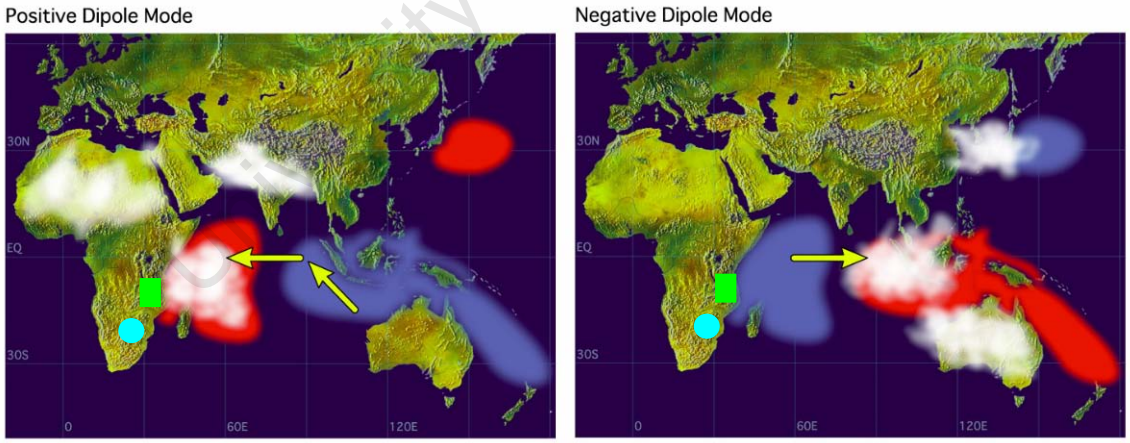

Figure 1.1 The surface temperature anomalies and wind direction during a positive (left) and a negative (right) IODZM event. Red shading show warming while blue shading signifies cooling. White patches indicate increased convective activity. The rectangle and circle represent the regions of northeast and southeast African rainfall. Image: courtesy of JAMSTEC IOD website, http://www.**jamstec**.go.jp/ frsgc/research/d1/**iod**/.

As we can see from figure 1.1, the east African region shares the same maritime rainfall with the western Indian Ocean, the physical location of the IODZM's western pole. This factor triggered several investigations to determine the IODZM forcing of the sub-regional rainfall immediately after the acknowledgement of the IODZM as a physical entity (e.g. Clark et al., 2003; Black et al., 2003; Hastenrath et al., 2004). This resulted in some studies suggesting that ENSO could be playing an insignificant role in the austral summer rainfall variability of this sub-region. For example, Yamagata et al. (2003) and Behera et al. (2005) insist on the paramount impact of IODZM over the northeast SADC. But over the southeastern region, only a few studies (e.g. Black et al., 2003; Saji and Yamagata, 2003) merely mentioned the IODZM potential impacts, but without due emphasis which normally accompanies a worthy regional discovery. It is Manatsa et al. (2007, 2008, 2010) and, Manatsa and Matarira (2009) who recently observed that the IODZM may dominate Zimbabwe rainfall variability. Consequently, it means that the IODZM could be driving essential rainfall impacts whose manifestations are opposite over East and Southern Africa. Thus the IODZM related rainfall causing mechanisms over the east SADC region could be considered as the possible explanation to the research by Jury et al. (2002), which concluded that the east African rainfall regime shares maritime convection with the Indian Ocean, while convection over southern Africa is inversely related. We therefore suggest that the current study can offer alternative explanations as to why presently, scientific advances in seasonal rainfall prediction skill are still limited to very modest levels in the eastern SADC region. At the same time, since this anomaly pattern involves rainfall extremes, its seasonal prediction has considerable applications for decision making in disaster management for the SADC region as a whole. This makes the understanding of this dipole rainfall phenomenon a regionally worthwhile issue, both socially and scientifically.

1.4 The Hypothesis

From the above argument, it emerges that one school of thought regards the northeast and southeast SADC rainfall as one and the same system dominantly controlled by ENSO (Nicholson and Kim 1997). Another view considers these rainfall regimes as relatively independent subsystems influenced by different climate modes (McHugh and Rogers, 2001). Evidently, there is a relatively large gap in the knowledge and understanding of the causes of the opposing rainfall anomaly pattern and the related prime teleconnections. At the same time, an unambiguous understanding of this eastern SADC's dipole like rainfall anomaly structure is clearly of scientific and social value. In our effort to offer a more viable alternative explanation, we first acknowledge the importance of mechanisms and processes which determine ENSO related variability and impact on SADC climate. However, this should not distract us from concentrating on the IODZM variability and the ensuing ramifications for regional climate, components of which are increasingly shown to be distinct from ENSO (Merchant et al., 2006). Thus contrary to the classical view that preserves ENSO dominance in the regional rainfall variability, we adopt a hypothesis that partially eclipses ENSO by significantly elevating the importance of the rainfall control emanating from the tropical Indian Ocean SSTs. We consider the IODZM as a largely independent climate mode that mostly evolves free of Pacific influence (Behera et al., 2005) but, whose mature phase strongly influences the developmental stages of ENSO during boreal fall in years of co-occurrence (Annamalai et al., 2004). The hypothesis is that, the east SADC early summer rainfall shows a dominant meridional dipole rainfall anomaly pattern which is essentially a manifestation of the influence of the adjacent IODZM phenomenon rather than the impact of the relatively remote ENSO.

1.5 The Scope of the Thesis

In this study, we adopt an approach of considering the IODZM as a significant air-sea coupled phenomenon unique to the Indian Ocean, but which at times is contaminated by other important tropically based climate modes such as ENSO (Behera et al., 2005). It is for this reason that understanding the teleconnection patterns related to IODZM and/or ENSO together with their positive/negative interferences during years of co-occurrence becomes very important. We therefore investigate the unique influence of IODZM and suggest that this new independent climate mode could provide some of the answers to the irregularities that were earlier referred to in the ENSO-SADC rainfall relationship. Thus this thesis is restricted to the mainland SADC region south of the equator (figure 4.1) and the period of study is from 1950 to 1999. In this region the northeastern sector experiences two different rainy sub seasons, the 'short rains' from October to December (OND) followed by 'long rains' from March to May (MAM). Similarly, the southeastern part also has two distinct sub seasons, the early summer during OND and the late summer season from January to March (JFM). It is the OND sub season for both subregions which has comparatively less rainfall total amount that is characterized by relatively much higher interannual variability (Clark et al., 2003; Richard et al., 2001). Since it appears that the earlier and later sub seasons in both regions are weakly linked, we only consider for analysis the OND sub season because it inherits a larger impact on the communities through changes in the regional hydrological cycle and is fairly less reliable due to its greater variability. We also deliberately underplay the role of the Atlantic Ocean, as the convective variability in this ocean is much weaker than either ENSO or IODZM (Xie and Arkin, 1996). However, this does not completely discredit the role of the Atlantic Ocean. There are currently arguments that this ocean may play a significant role in the SADC rainfall teleconnection (Rouault et al., 2003, 2005; Reason

et al., 2006). Even, Nicholson and Kim (1997) were quite convinced that the Atlantic Ocean plays a more essential role in governing rainfall over the eastern SADC than does the Indian Ocean. Thus this study attempts to bridge the glaring gap in the understanding of the east SADC opposing rainfall anomalies, in an effort to improve seasonal rainfall forecasting.

1.6 Scientific Objectives

The aim of this thesis is to use observational data to demonstrate that the dominant early summer rainfall variability pattern over the east SADC region is a meridionally aligned dipole rainfall anomaly pattern whose southern pole is positioned over south east Africa and the northern pole is situated over east Africa. But most importantly, to provide evidence that this rainfall configuration is mainly related to the adjacent IODZM rather than the influence of the relatively remote ENSO.

1.6.1 Specific Objectives

- To demonstrate that the dominant rainfall variability for the early summer period over the east SADC region is an opposition in rainfall anomalies with one node over the northeast (east Africa) and the other over the southeast (southern east Africa).
- To investigate the spatial and temporal extent of the opposing rainfall anomalies.
- To show the dominance of IODZM influence over ENSO in the association to the meridional dipole rainfall pattern through partial correlation analysis
- To illustrate the paramount participation of the IODZM events in co occurring with the meridional dipole rainfall anomaly pattern using the pure composite analysis.

- To investigate the temporal stability of the superior role of IODZM in the relationship with the meridional dipole rainfall anomaly configuration during the study period.

1.7 Structure of the Thesis

Section 2 is devoted to the data descriptions and section 3 to the methods used in the thesis. In chapter 4 we show that the dominant rainfall variability for the early summer period of eastern SADC region assumes a meridional dipole like pattern. We further provide evidence to support the dominant participation of the IODZM rather than ENSO in the development of this dipole rainfall pattern. Section 5 is devoted to the summary and discussions.

CHAPTER 2:

Data

This study uses four time series for the period 1950 to 1999 in the investigations. The ENSO and IODZM SST time series are derived from the respective Niño 3.4 and IODZM regions. The rainfall time series are for the early summer rainfall of the two regions located over the northeast and southeast of the SADC region.

2.1 ENSO and IODZM index.

2.1.1 Niño 3.4 index

ENSO signal, as depicted by eastern equatorial Pacific SST anomalies, is indexed by the familiar Niño 3.4 SSTs in this study. This index is well correlated to other ENSO indicators (Camberlin et al., 2001) and has been used in several studies to determine the impacts of the eastern Pacific on the African rainfall (e.g. Clark et al., 2003; Mapande and Reason, 2005; McHugh, 2006). It is calculated by taking the average of SST anomalies over 5^0N - 5^0S, 170^0W – 120^0W (see figure 2.3). The observed SST anomalies are computed from the Hadley Centre sea ice and SST (HadISST) data set (Rayner et al., 1996)**.** The Niño 3.4 index is preferred over the Southern Oscillation Index (SOI) as it represents the ENSO phenomenon more compactly (Soman and Slingo, 1997). This SST index makes it easier for comparison purposes with the IODZM index that is also SST based. In this thesis the Niño 3.4 index is adopted as the average of October to December (OND) SST anomalies. This is the period when the ENSO influence has been found to project its maximum impact on the early summer rainfall of the region as compared to other lagged periods. The index is normalised relative to its

standard deviation. Figure 2.1 shows the temporal evolution of amplitude variations of the Niño 3.4 for the period 1950 to 1999. The El Niño events are considered as anomaly values outside the ±0.7 threshold, which has been demarcated by the solid lines above and below the x axis respectively. This standard deviation criterion extracts 12 El Niño events and 14 La Niña events.

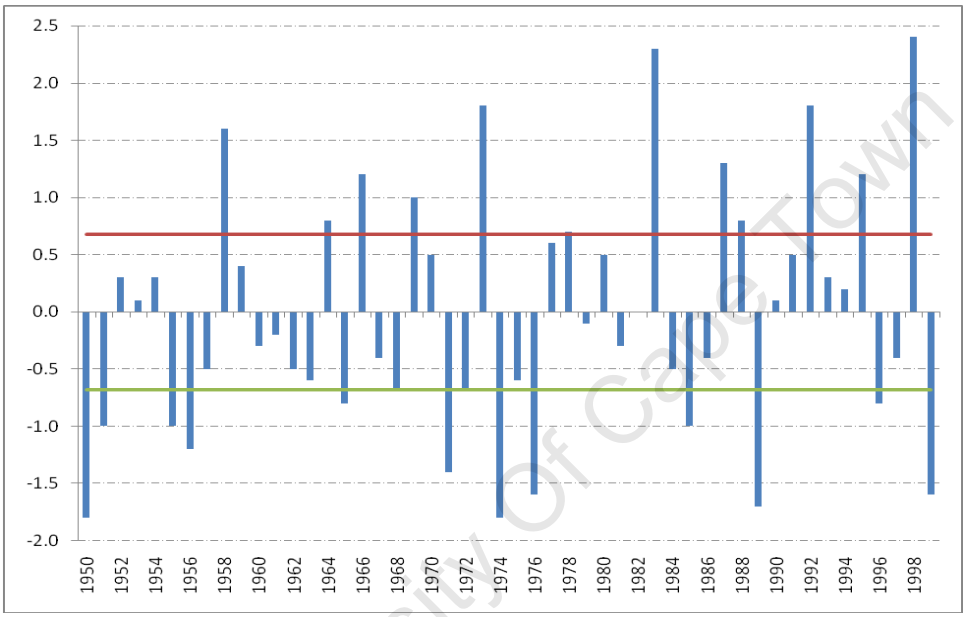

Figure 2.1 Bar charts for the OND mean of the Niño 3.4 index for the period 1950-1999. Horizontal solid lines show the threshold of ±0.7 for the warm ENSO phase (El Niño) events (upper solid line) and cold ENSO phase (La Niña) events (lower solid events).

2.1.2 Indian Ocean Dipole/Zonal mode Index (IODZMI)

The Indian Ocean Dipole/Zonal mode which is sometimes referred to as the Indian Ocean Dipole Mode (Saji et al., 1999, Behera et al., 2005, Yamagata et al., 2003) represents the dominant climatic mode found in the tropical Indian Ocean. Its strength is measured through the IODZM index which quantifies zonal gradients in the SST rather than the proper east-west dipole. Thus we opted to use the term IODZM (as used by

Annamalai et al., 2004 and Clark et al., 2003) as it matches the observed out of phase rather than the simultaneous variations in the development of the SST extremes in the east and west of the Indian Ocean (Clark et al., 2003). As a result this definition may include some of the noted anomalous years (e.g. 1972, 1986 and 1991) that are linked to strong zonal gradients in the SST rather than the proper east-west dipole. Following Saji et al. (1999), we considered the IODZMI as the anomaly difference between the SST anomalies of the western (50^0E –70^0E, 10^0 S-10^0N) and eastern (90^0E-110^oE, 10^0S-Eq) tropical Indian Ocean (figure 2.3). The SSTs for the IODZMI dataset (from 1940 to 1999) were adopted from Kaplan (1998) and extracted from http://www.jamstec.go.jp/frcgc/research/d1/iod/ kaplansstdmi.txt. The IODZMI is calculated from the average of the most active months of September to November (SON) and normalised relative to its standard deviation. For the sake of consistency we also adopted ±0.7 as the value above/below which defines the positive and negative IODZM events. In this way, 12 positive and 15 negative IODZM events are extracted from figure 2.2.

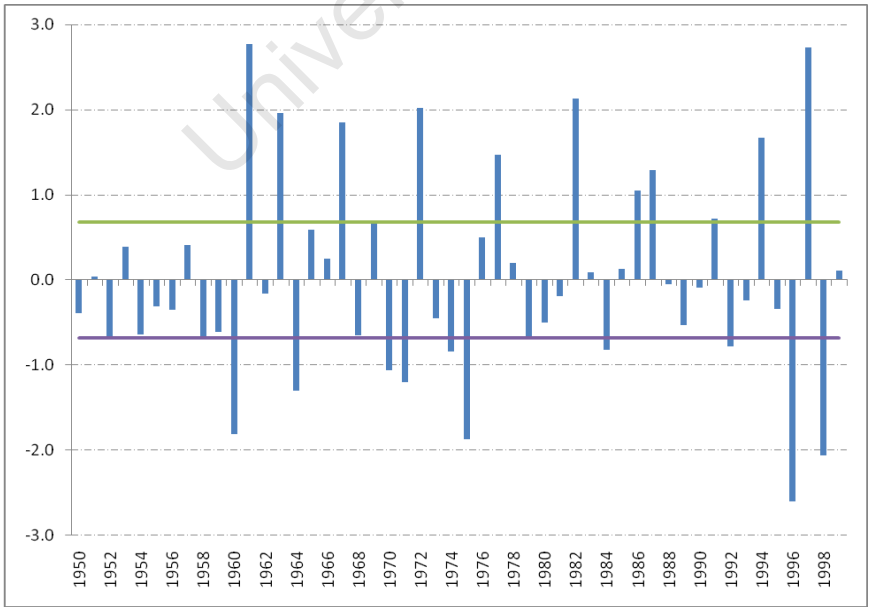

Figure 2.2 Bar Charts of the SON mean of the IODZMI for the period 1950-1999. Horizontal solid lines show the threshold of ±0.7 for the positive IOD events (upper solid line) and negative IODZM events (lower solid line).

Note that the El Niño (positive (p) IODZM) and La Niña (negative (n) IODZM) event are defined as those values exceeding positive and negative 0.7 standards deviations from the respective means. This threshold value, although not standard, has been deliberately chosen as it is the level that has been shown to favour anomalous rainfall events over southern Africa (Manatsa et al., 2008). At the same time, these event phases match closely those that are widely used as proposed by Yamagata et al. (2004). The events are categorized as either pure or co-occurrence. A p(n)IODZM event is considered as pure IODZM event when El Niño (La Niña) does not occur at the same time with it. Similarly El Niño (La Niña) event is considered a pure event when it does not co-occur with a p(n)IODZM event. When the p(n)IODZM and El Niño (La Niña) events occur at the same time, the situation is considered as a co-occurrence event. Using this classification the study period has no concurrent events with opposite phases. Table 1 shows the classification of these ENSO and IODZM event years.

Table1. Classification of ENSO (averaged OND SSTs) and IODZM (averaged SON SSTs) events from 1950 to 1999

Pure nIODZM	Pure La Niña	Pure pIODZM	Pure El Niño	Co-Occurrence El Niño & pIODZM	Co-Occurrence nIODZM & La Niña
1952	1950 1983	1961	1951	1963 1991	1964 1998
1960	1954 1988	1967	1957	1969 1994	1970
1979	1955 1995	1977	1965	1972 1997	1971
1992	1956 1999		1976	1982	1974

1996	1962	1986	1975
	1973	1987	1984

2.2 Spatial Indo-Pacific SSTs

The spatial and temporal associations of rainfall indices with SSTs in the tropical Indo-Pacific region are done only for the available data for the period from 1951 to 1999. The Indian Ocean and Pacific SSTs processed files are downloaded from NOAA ftp site. The spatial sea surface temperature data is extracted from the area bounded by latitude 33^{0}E to 70^{0}W and longitude 20^{0}N to 30^{0}S (area shown in figure 2.3). The mapping of the correlation coefficients between regional rainfall indices and Indian Ocean SSTs in the tropical Indian Ocean/Pacific (figures 4.6 a and b) is done using ClimLab 2000 software.

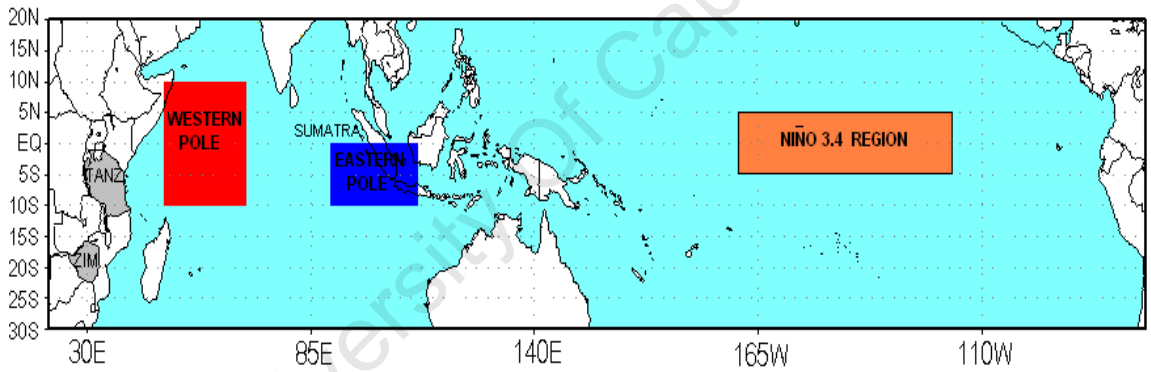

Figure 2.3. Map showing the regions where IODZMI and ENSO SST data for the analysis were extracted. The magnitude of the IODZM is represented by the standardised SST difference over the western and eastern poles as shown in the shaded blocks in the Indian Ocean. Niño 3.4 SST region is shown by the box in the equatorial Pacific Ocean.

2.3 Rainfall Data

The rainfall data are derived from University of Delaware gridded high resolution precipitation dataset. Using the statistical technique described in Willmott and Mutsuura

(1995), the University of Delaware team interpolated the precipitation data from archives of Legates and Willmott (1990). The dataset covers the period 1950-1999 and provides 0.5^0 latitude–longitude grid interpolated data of observed land only rain-gauge based monthly total precipitation fields. The anomalies are derived from long term means from 1950 to 1999. For a complete description of the data set, see web pages at http://climate.goeg.udel.edu/~climate. Although the reliability of the observed rainfall data over much of the region, especially in the lower latitudes is questionable, it is considered as the best free and readily available data over the region (Reason and Jagadheesha, 2005). We adopt for analysis the SARCOF's definition of early summer rainfall season which spans from October to December (OND).

The regional rainfall time series for the two coherent areas identified through Empirical Orthogonal Function (EOF) analysis, have been prepared from the boxes with the highest positive loadings [33^0E to 38^0E; 6^0S to 11^0S] over north east SADC and lowest negative loadings [28^0E to 33^0E; 20^0S to 25^0S] over south eastern SADC. We see that the northeastern region covers central eastern Tanzania and the southeastern region includes the Limpopo drainage sector of southern Zimbabwe, northern South Africa, eastern Botswana and southwest Mozambique (see figure 4.2). In this way the rainfall index for northeast SADC OND rainfall (NESOR) and southeast SADC OND rainfall (SESOR) is constructed for the regions and designated them as NESOR index and SESOR index respectively. In forming these indices, the gridded point rainfall time series were normalized by dividing their seasonal (OND) departures from the long term mean by the seasonal standard deviation. These standardized time series for each grid point were then aerially averaged according to their respective regions in order to ensure that all locations contribute equally to the regional indexes as per Jones and Hulme (1996). This methodology also filters out noise produced by strong interannual localized climate

regimes common across these areas and retains only commonalities. The temporal manifestations of the two indices NESORI and SESORI are shown in figure 2.4 and 2.5 respectively. The high variability of the two time series is quite evident in the graphs. It can also be noted that there seem to be an inverse link between the two time series as in many years, high amplitude negative bars coincide with large positive bars and the reverse. It is on the basis of this finding that the common Chi Square (χ^2) test is employed to test the significance of this inverse connection between NESORI and SESORI.

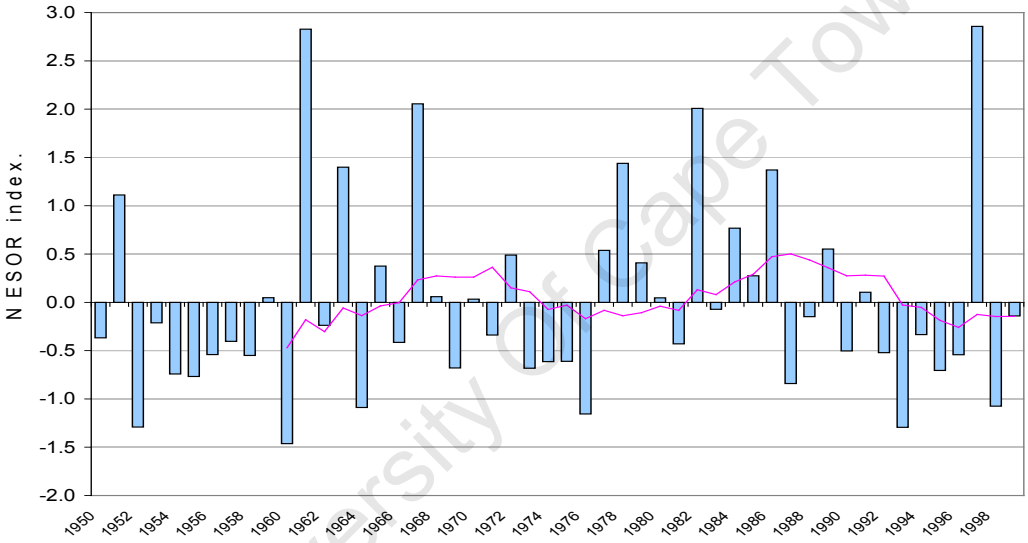

Figure 2.4. The temporal variability of NESORI for the period 1950 to 1999. An 11 year running mean is inserted with values read at the end of the 11 year segment.

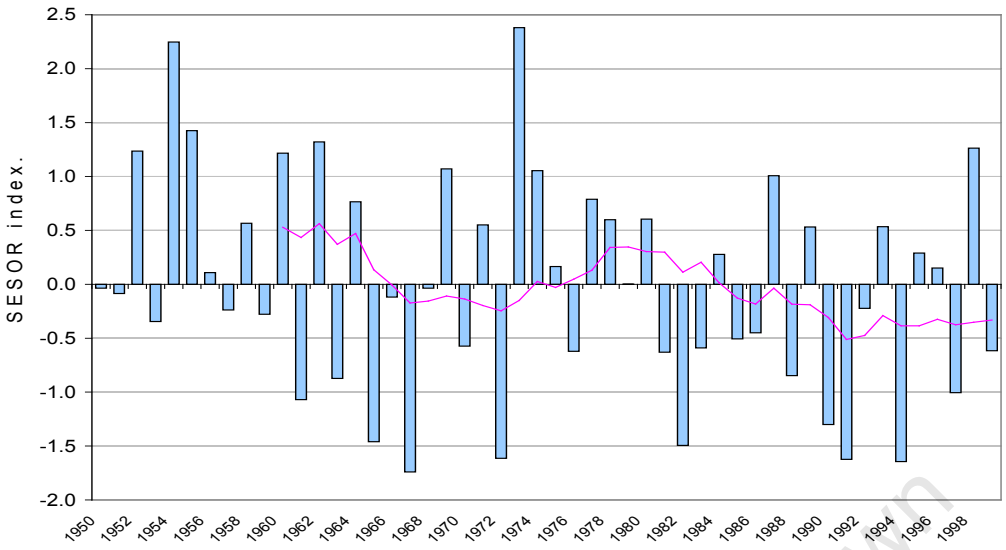

Figure 2.5. Same as figure 2.4 but for the southeast OND rainfall index (SESORI)

CHAPTER 3:

Methods

The study relies heavily on linear statistical tools in the analysis. This is because the SSTs and rainfall time series have been found to be largely normal, making linear assumptions in relationships appropriate. Also we believe the statistics of the climate are generally captured, to a good approximation, by linear analysis. Composite techniques were used as a complement. Spatial relationships are determined and mapped through simple correlation analysis with OND rainfall total at each grid point. To show the possible fractional influences of ENSO and IODZM, we used the partial correlation technique. Although there are a number of limitations to this methodology, most notably related to linearity, it does provide a basic way of analysing variability of ENSO (IODZM) independent of IODZM (ENSO). This approach has been used in a number of previous studies for the same purpose (e.g. Behera et al., 2005, Yamagata et al., 2004; Saji and Yamagata, 2003). Pure composite analysis is also used to segregate influences unique to each of the two climate modes. In order to diagnose changes and quantify the

decadal variability of ENSO, IODZM, NESOR and SESOR indices, their respective windowed running time series (values calculated in successive windows) were created. But to gain the temporal sense among the relationships, 31-year running correlation analysis is used. These correlations, computed in 31-year moving windows necessitate the determination of the consistency including the time location of the correlation coefficients, (e.g. Haylock et al., 2007; Saji and Yamagata, 2003; Behera et al., 2005) and allows diagnosis of changes in relationships as well as detecting low frequency variations in the interactions. This window width of 31 years was adopted, not only to conform closely to the World Meteorological Organization's standard climate period of 30 years, but most importantly, we noted that the measures of the moving mean, variance and correlation coefficients start to stabilize after a 31-year period. For example, when we reduced the period length, (e.g. 21, 11 and 5 years) these measures became too fluctuating and consequently, the representativeness of the variability was quite weak. Thus throughout the study we opted for the 31 years as the segment period of analysis and indicate time by end year rather than the usual center of the period (Parthasarathy et al., 1991 and Richard et al., 2001). Although this is not a popular graphical data presentation method, it has the advantage of allowing for the direct determination of the impact of the contribution of the ending year value to the process being investigated. Thus the impact of including the 1997/98 year value in the 31 year segment is reflected directly above the year 1997/98.

3.1 Partial Correlation

To show the independent influence of the IODZM/ENSO on seasonal rainfall, we employed the partial correlation technique as used by Saji and Yamagata (2003), Behera et al. (2005) and Ashok et al. (2004). In this approach, the exclusive relationship between two variables can be realized while excluding the influence arising from another

independent variable (Behera and Yamagata, 2003). For example the partial correlation between NESORI and IODZMI, while excluding the relation arrived at because of the correlation between ENSO and NESORI, is defined as follows:

$$r_{nesori\ \&\ iodzmi,\ nino3.4} = \frac{r_{nesori\ \&\ iodzmi} - r_{nesori\ \&\ nino3.4} \times r_{nino3.4\ \&\ iodzmi}}{\sqrt{1 - r^2_{nesori\ \&\ nino3.4}}\sqrt{1 - r^2_{nino3.4\ \&\ iodzmi}}}$$

Where $r_{nesori\ \&\ iodzmi}$ is the correlation between rainfall anomalies and IODZMI,

$r_{nesori\ \&\ nino3.4}$ is the correlation between rainfall anomalies and Niño 3.4 index,

$r_{nino3.4\ \&\ iodzmi}$ is the correlation between rainfall anomalies and IODZMI.

Similarly, the partial correlation is obtained for Niño 3.4 and precipitation anomalies while excluding the influence due to the correlation between IODZM and precipitation anomalies.

In addition to the length of the indices, it has to be noted that the statistical significance of cross correlations, be it partial or simple, also largely depends on the auto correlation characteristics and smoothing of each time series involved. In this thesis there is no prior smoothing of time series used in the cross correlation coefficients presented neither were there any time filters applied to any of the above data sets to remove periodic variations. Moreover, the coefficients are also based on yearly sampled series (i.e. the time interval between two observations is one year) thus showing insignificant lag-1 auto-correlation (e.g. Terray et al., 2005). This made it appropriate for us to evaluate the statistical significance of our correlation coefficients by the standard two tailed t-test.

3.2 Pure Composite Analysis

We use pure composite analysis as used by Ashok et al. (2004) to elucidate the independent large scale impact of ENSO and IODZM events on SADC rainfall. The composite plots are constructed based on combinations shown in Table 1. To form the composites fields for each category, rainfall anomalies are calculated as the deviation of the composite seasonal rainfall mean from the long term seasonal mean (1950 to 1999). In total 4(10) pure El Niño (La Niña), 3(5) pure p(n) IODZM events and 9(7) co-occurrence El Niño-positive IODZM (La Niña-nIODZM) events are used to prepare the composite pictures. The total number ensures robustness of the results. It is noted however, that only three pure pIODZM events can be classified during the study period. This renders the reliability of this particular composite sample a concern. It has to be also noted that the frequency of pure El Niño is less than half that of La Niña (4 out of 10). Similarly pure pIODZM events occur less than the nIODZM events, 3 out of 5 cases.

By analyzing the general composite properties, prominent features of selected years are enhanced, while noise present in individual events is mostly removed. Since the maps that we constructed show raw composite rainfall anomalies, they tend to be large where the mean seasonal precipitation is highest (towards the north, figure 4.1). At the same time, the anomalies do not appear large or are absent altogether over the southwest (mostly over the desert) where the mean precipitation is relatively low compared to the rest of the SADC region. Normalizing the anomalies would have solved the problem but we preferred to bring out the actual rainfall deviation amounts for better presentation of our arguments.

Significant composite anomalies were thus assessed through performing a local two sample student's t-test on every grid point. The t-test statistics of this procedure are given by the following formular:

$$\frac{(\mu_1 - \mu_2)}{\sqrt{\frac{\delta_1^2}{n_1} + \frac{\delta_2^2}{n_2}}}$$

where μ_1 and μ_2 are the means, δ_1 and δ_2 are the standard deviations and, n_1 and n_2 are the number of events in sample 1 and sample 2 respectively. Sample 1 is he composite being investigated while sample 2 is the overall period under study. Briefly, this method determines the areas in the composites that depart significantly from the background variability in the available data. The SURFER (1997) software was then used to join points of the 5% and 10% significance threshold level. In this way, we were able to define regions within the composite anomalies that depart significantly from the background variability (shaded grey in respective figures) in the OND SADC rainfall region.

3.3 Regionalization by Empirical Orthogonal Functions (EOF) analysis

The Empirical Orthogonal Functions Analysis (EOF) also known as Principal Component Analysis (PCA) is a multivariate technique widely used in meteorology and climatology. It was first introduced by Pearson (1901) and further developed by Hotelling (1933). It involves a mathematical procedure that attempts to transform a large number of highly inter-correlated variables into a smaller number of uncorrelated variables called principal components (PC scores) and consist of linear combinations of the original variables. The coefficients of the linear combinations are called 'loadings' and represent the weight of the original variables in the PCs. That is why the results of a PCA are usually discussed

in terms of component scores and loadings. The factor loadings tell us about the spatial patterns while each PC indicates the fraction of the total variance explained by each factor loading. The cases or PC time series indicate the amplitude of the PC with time. In this way, regions can be defined where for any point within each region, the rainfall time series co-varies. It has to be noted that the PCs with the largest eigenvalues (dominant principal components or PC1) correspond to the dimensions that have the strongest correlation in the data set.

This dimension reduction technique can lead to a more tractable understanding and interpretation of the gridded rainfall data set. Often, its operation can be thought of as revealing the internal structure of the data in a way which best explains the variance in the data. It has the advantage that the resulting patterns are considered as orthogonal modes of variability. In applying this method, we derive a relatively smaller number of factors that can be used to represent relationships among sets of multiple interconnected grid point rainfall time series. The first principal component accounts for as much of the variability in the data as possible, and each succeeding component accounts for as much of the remaining variability as possible. In this way we can extract condensed information from the multiple and noisy time series that may provide us with insights into the unknown or partially known dynamics of the underlying system that generates the particular series and patterns. Hence we are able to delineate subregions where strong and coherent spatial and temporal correlations prevail within the OND rainfall time series located at multiple grid points over the selected eastern SADC region (23^0E to 40^0E and equator to 30^0S).

But after studying extensive literature on PCA (Richman, 1986; Joliffe, 1986, 1987, 1990; White et al., 1991) we note that this method also inherits some limitations. The

major one being that the unrotated PCAs have a tendency to produce expected patterns. The first component maximizes the explained variance by having generally large loadings on all the variables and hence subsequent patterns are dipole or more complex patterns. Buells (1975) for example has some reservations on the interpretation of unrotated PCs. He noted that they may not capture the nature of the well known correlation functions. This means that the direct interpretation of the unrotated PCs can thus be misleading and rotating these is regarded as one possible solution to this problem.

Hence, in order to facilitate the interpretation of the spatial analysis of the factor loadings, it became necessary to rotate the axis. We chose the process that achieves discrimination among the loadings but keeping the factors uncorrelated. The applied process is called Orthogonal Varimax Rotation (the algorithm used is FROTA, IMSL., 1987). Obviously, each rotated pattern will not explain the same variance of the unrotated principal components although the total variance of the explained remains the same. Details of this principal component analysis method can be obtained in any standard statistical textbook (e.g. Wilks, 2006).

However, in general, there is no guarantee that these evaluated factors represent dynamically existing entities, as with any statistical tool. Thus it is important to determine whether or not these results have any physical meaning. The basic assumption is that the underlying dimensions or factors can be used to explain complex meteorological or other climatological variables. In the current study we only extracted the factor loadings of the dominant principal component (PC1) for spatial interpretation through plotting using SURFER (1997) software. This exercise is assumed to have revealed the dominant rainfall variability pattern of the eastern SADC region during the OND period.

3.4 Wavelet Power Spectrum Analysis

Since the time series for ENSO, IODZMI and the OND SADC rainfall exhibit non-stationarity in their statistics, they may contain dominant periodical signals that can vary in both amplitude and frequency over the 50 year period. These can be compared to determine similarities and differences especially in analysing the cause effect behaviour that can be suspected between time series. We opted for the global wavelet power spectrum (GWS) analysis technique using the Morlet wavelet to extract these variations. This GWS provides unbiased and consistent estimation of the true power spectrum of the time series thus a simple and robust way to characterise the time series (Santos et al. 2001).

This method is able to decompose a time series into time/frequency space simultaneously and hence provide information on the amplitude of the periodic signal within the time series and how the amplitude varies with time. We applied zero padding to reduce wraparound effects (Torrance and Compo 1998), but this has an effect of reducing the spectral peaks near the edges. Since the null hypothesis for the wavelet assumes the mean power spectrum (global wavelet spectrum), when a peak in the wavelet power spectrum is significantly above the background spectrum, it is therefore assumed to be the true feature with a degree of significance (Behera and Yamagata 2003). This means that the 90% confidence level is the 90^{th} percentile of the background spectrum. Details of the wavelet method and the determination of significance are discussed in Torrance and Compo (1998).

CHAPTER 4:

Results

4.1 The East SADC Rainfall and its Spatial Coherence

It is necessary to first appreciate the spatial distribution and temporal variability of the rainfall so as to understand the spatial extent and temporal pattern of the IODZM and/or ENSO influence on SADC seasonal rainfall. The spatial distribution of the rainfall is determined by the mean seasonal rainfall at the grid points provided by the dataset. The mentioned concerns on the gridded data render the validation of the dataset necessary. Thus in figure 4.1 we present the OND monthly mean rainfall over the SADC and compare it with Map C for October to December SADC rainfall from http://www.dmc.co.zw/SARCOF/SarcofStatementSep2003Lusaka.pdf, that has been directly constructed from rainfall based on SADC Meteorological Services datasets. These two rainfall maps compare favorably and thus warrant the adoption of the readily available University of Delaware gridded high resolution precipitation dataset as a viable option for use in this study.

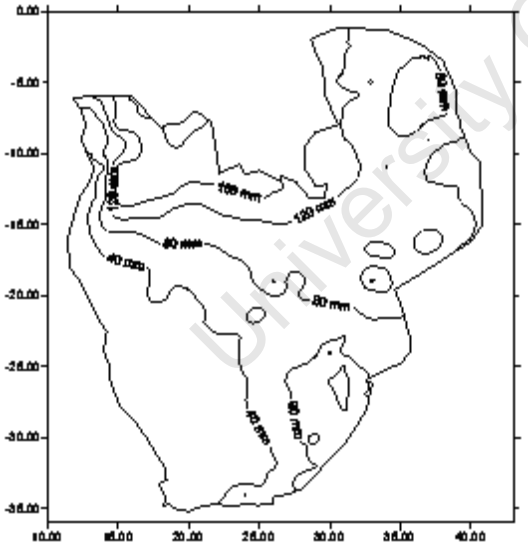

Figure 4.1. Spatial distributions of October to December SADC mean monthly rainfall (monthly rainfall data is from University of Delaware)

To have a closer look at the spatial coherence of the mean OND rainfall of the eastern SADC region, precipitation time series at the grid points falling between the equator and

the 30^0 S latitude and 23^0 E to 40^0 E were subjected to EOF analysis. But a major problem with this method is that unrotated EOFs have a tendency to produce predictable patterns (Richman, 1986). In this instance we therefore complemented the unrotated with the rotated procedure of this technique. However, there was not much deviation of the second outcome from the first result. We found that one of the most outstanding characteristics emanating from this dual operation is that the OND precipitation shows a remarkable degree of spatial coherence. This can be deduced from the spatial manifestation of both the unrotated (figure 4.2a) and rotated (figure 4.2b) leading principal component (PC1). The rotation was done using the VARIMAX rotation method and as already alluded to, this was a supplementary step specifically designed to further refine the initial unrotated EOF analysis.

Qualitatively similar PC1 loading patterns were observed when the unrotated and the varimax rotated solutions were compared though they explained 37 % and 31 % of the OND rainfall variance respectively. Besides demonstrating high coherence among the rainfall anomalies over the east SADC, the pattern indicates the existence of opposite PC loadings with an unequal, yet distinct north south orientated 'dipole'. The loadings are much stronger in magnitude (twice as much) over the northeast than over the southeast. This implies that rainfall anomalies of opposite sign tend to be found on either side of the zero PC1 loading contours (figure 4.2), with the northern region having more coherent rainfall anomalies than its counterpart to the south. These high value but opposite loadings over east SADC are consistent with Janowiak (1988). We then define the two regions having the high PC loadings as boxes whose locations are shown in figure 4.2 and designate them as south east SADC OND rainfall region (SESOR) and north east SADC OND rainfall region (NESOR).

This procedure of regionalizing rainfall variability using the multivariate technique provides the framework for the thesis. We note that the most relevant aspects of rainfall variability for this study are in fact the spatial patterns and spatial scales of rainfall anomalies in the early summer period of the sub region. Most interesting is the observation that in literature related to spatial rainfall patterns the world over, one can hardly identify adjacent regions where interannual rainfall variability is not only so spatially coherent but uniformly opposite in sign. Perhaps the closest could be the meridional dipole rainfall over West Africa described in Nicholson and Webster (2007). However, due to this exceptionally strong coherence of the OND rainfall anomalies, we found it appropriate to describe the rainfall variability in the eastern SADC region using aerially averaged NESOR and SESOR time series. The respective rainfall indices were then derived from these time series using the method described in section 2.

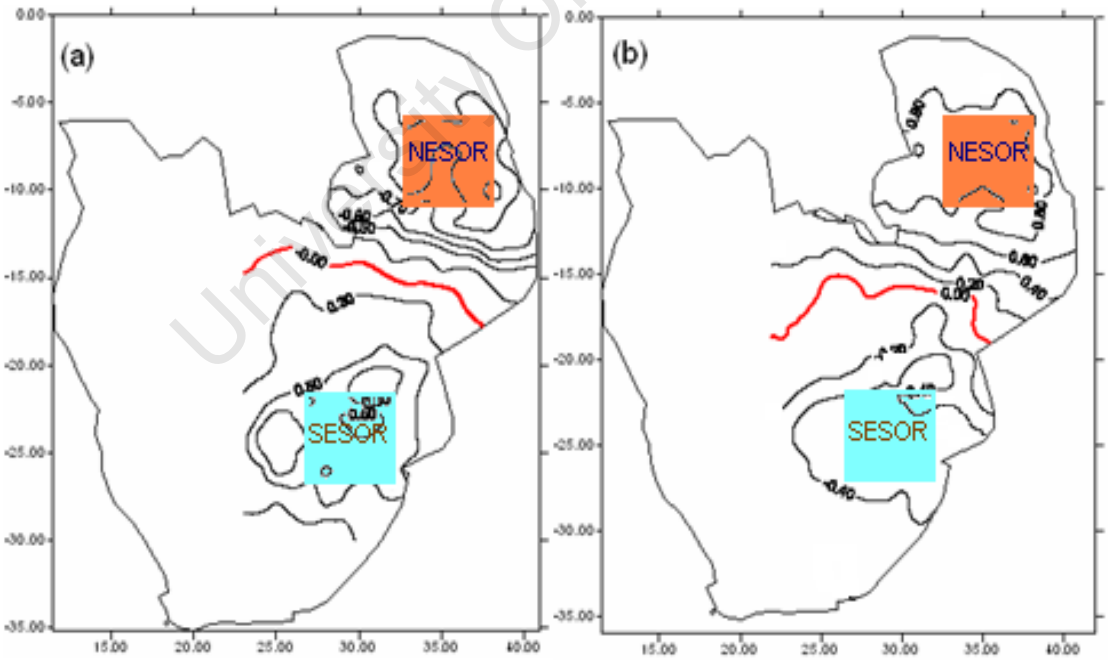

Figure 4.2. East SADC (a) unrotated and (b) rotated factor loadings for PC1 of the period 1950 to 1999. Boxes represent NESOR and SESOR regions where the respective rainfall indexes have been derived.

It is important to note that the structure of opposing factor loadings is defined by the same principal component (PC1). This may mean that they form a dipole by varying simultaneously as part of one principal component making. It is therefore most likely that these two homogeneous regions may be in response to only one ocean-atmospheric coupled mode or at least very closely related modes. However this observation contradicts the work of McHugh and Rogers (2001) who found that the rainfall anomalies for the two regions are part of two different principal components, south eastern part being linked to ENSO while the northern east is associated with NAO. At the same time they confirmed that NAO is weakly related to ENSO. These differences may be attributed to the fact that McHugh and Rogers (2001), analysed the December-January-February period while we concentrate on the OND period.

As would be expected from the leading PC loading patterns discussed above, the most obvious aspect to expect is that the SESORI is strongly out of phase with NESORI. Thus we also investigated if the opposing dominant principal component factor loadings noted above also translate into significant opposite relationships between NESOR and SESOR. A simple correlation analysis performed between these two time series yields an overall negative value of -0.53 which is significant above the 99% confidence level. This significant inverse relationship clearly occurs throughout the 31 segments of the study period albeit with gradually declining intensity and significance; reaching 95% confidence levels towards the end of the 20th century (see figure 4.13). Thus since the connection between NESORI and SESORI is strongly inverse, then the extreme events of either drought or floods should rarely occur simultaneously over the two regions but

deficit rainfall over one region should occur concurrently with excess rainfall over the other and vise versa.

An investigation into the yearly rainfall anomaly spatial distribution revealed that the node of this opposition in rainfall anomaly pattern is located around 15º S to 17º S. The transition along this latitudinal zone is so abrupt that in many years, the grid rainfall anomalies are almost uniformly signed be it north or south of this zone. But there exist another pattern though is relatively less frequent, the one that is characterized by anomalies of the same sign reflecting relatively mild dryness/wetness across both regions. However the later scenario is even less common. The net result is shown by way of a scatter plot depicting each of the four distinct configurations of rainfall anomalies in their respective quadrants, in figure 4.3. This scatter diagram (figure 4.3) illustrates better the simultaneousness of the extreme opposite rainfall events together with the relatively rare occurrences of the extreme rainfall of the same sign. Here we note a little more of co occurrence events of the combination when the rainfall is surplus over south-east Africa and deficit over east Africa in the fourth quadrant (35%) than in the second quadrant (33%) which represents the simultaneous occurrences but in the reverse. The combination in the first (10%) and third (22%) quadrants is dominated by relatively mild events where we see that the least frequent case when rainfall occurred with the same sign in both regions is located in the first quadrant. Thus it is quite apparent from this figure that the most common configuration is a dipole. This hypothesis can be strengthened by using the Chi Square (χ^2) test for testing the independence of two attributes. This is very important to know for socio-economic reasons over the SADC regional economic block, if severe droughts and flood conditions over these geographically separated regions alternate in their occurrence. This is examined in the following section.

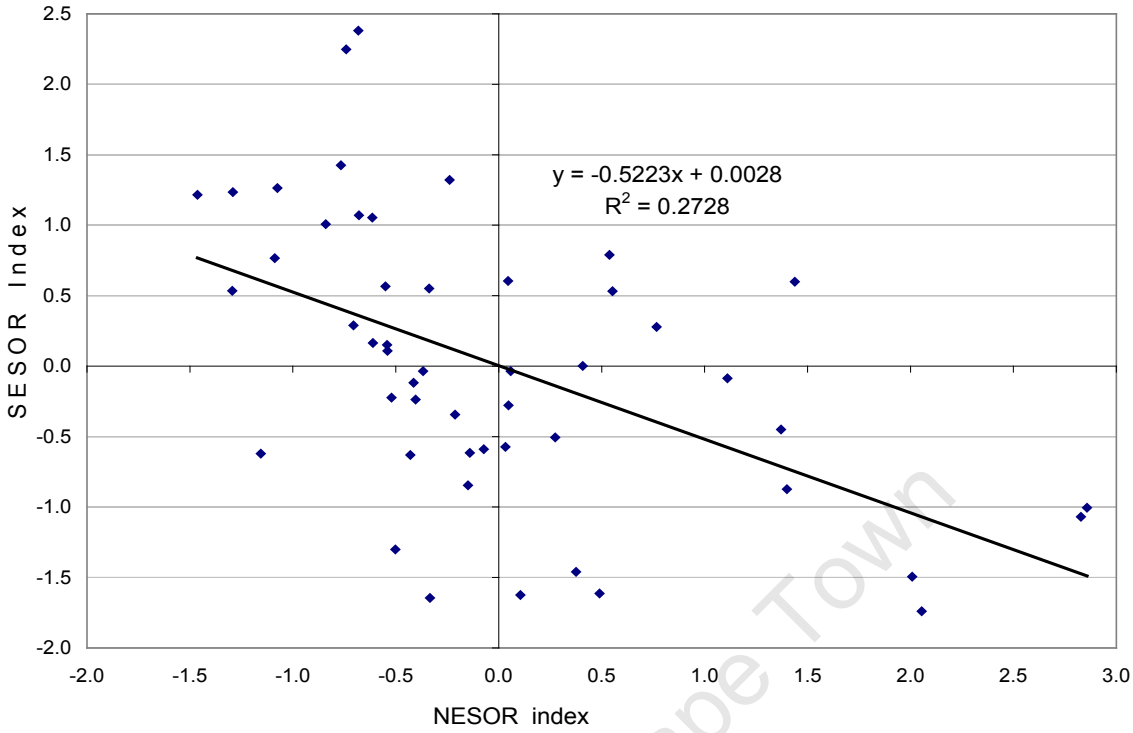

Figure 4.3. Scatter diagram showing the relationship between SESORI and NESORI for the period 1950 to 1999. The regression line/equation and the coefficient of determination are in the insert.

4.2 Chi Square (χ^2) test of significance between NESORI and SESORI

Since the χ^2 test uses the data that has been expressed in frequencies, it was necessary to first reduce the NESOR and SESOR indexes into four categories, ranging from greater than +1 (flood or excess rain), less than -1 (drought or deficit rainfall), between 0 and +1 (normal on the positive) and between -1 and 0 (normal but on the negative side). Based on these categories, a contingency table for the observed frequencies were prepared as shown in Table 2. From these observed frequencies, expected frequencies and the χ^2 value were computed by the usual procedure. In the contingency table provided in Table 2, the null hypothesis was that there is no relationship between the two variables i.e. the expected values in the rows and columns are independent. An analysis of the table shows that the χ^2 for the rainfall frequencies is 26.38, with a p-value of

0.0017. In this way, the null hypothesis of no relationship has to be rejected in favor of the existence of a strong inverse relationship. This implies that on more than 99.9% of the occasions, there is the likelihood that the simultaneous OND rainfall anomalies over northeast and southeast SADC would be different.

Table 4.2: Contingency table for observed frequencies of NESORI and SESORI categories. The expected frequencies are in brackets.

	NESORI	< -1	-1 to 0	>0 to +1	> +1	Total
	< -1	0 (1.68)	4 (3.12)	0 (0.72)	2 (0.48)	6
	-1 to 0	1 (5.32)	13 (9.88)	3 (2.28)	2 (1.52)	19
SESORI	>0 to +1	9 (5.88)	9 (10.92)	3 (2.52)	0 (1.68)	21
	> +1	4 (1.12)	0 (2.08)	0 (0.48)	0 (0.32)	4
	Total	14	26	6	4	50

$\chi^2 = 26.38$ *P-value* = 0.0017

A closer scrutiny of Table 2 also reveals that there is virtually neither a case when the NESORI and SESORI were simultaneously less than -1 (co-occurring droughts) nor a case when both rainfall anomalies coincided above the index value of +1 (concurrent excessive rainfall). While a strong SESOR rainfall anomaly (SESORI > 1) did not co-occur with any surplus NESOR event, there was only one case when an intense drought over east Africa (NESORI < -1) concurrently occurred with a normal but negative SESOR event. In fact most of the rainfall anomalies occurred with opposing signs, which strongly suggests a see saw behavior between east and south east African rainfall. Thus the regions of opposing factor loadings noted before are realistic in both a physical and statistical sense, and are not direct consequences of the application of the EOF method itself. This result in itself is an interesting finding and obviously a detailed analysis of the

OND rainfall over such significant coherent regions has been lacking. In the following sections we therefore subject the NESOR and SESOR series to simple statistical techniques in order to investigate their variations and teleconnections on interannual and decadal time scales.

4.3 Interannual and Decadal Climate Variability of NESOR and SESOR

The temporal comparison between the rainfall characteristics of these two regions is useful. In figure 4.4 we compare the linear descriptions of the two rainfall series through box and whisker plots. There are similarities between the monthly mean rainfall of the two regions. The medians are quite close, being 75.9 mm and 82.6 mm for SESOR and NESOR respectively. Although the monthly mean for NESOR is slightly more than that of SESOR by about 7 mm, the difference is not statistically significant (p-value = 0.29). However, NESOR has a standard deviation which is twice that of SESOR (17.0 mm compared to 33.3 mm), thus making NESOR acquire a coefficient of variation (44.5%) that is also almost double that of SESOR (22.8%). This suggests that the amplitude and the interannual variability are much larger for rainfall over the northeast than for southeast SADC. The same can also be inferred through the range of the monthly rainfall which is around 70 mm for SESOR but that for NESOR is about twice as much, 144 mm.

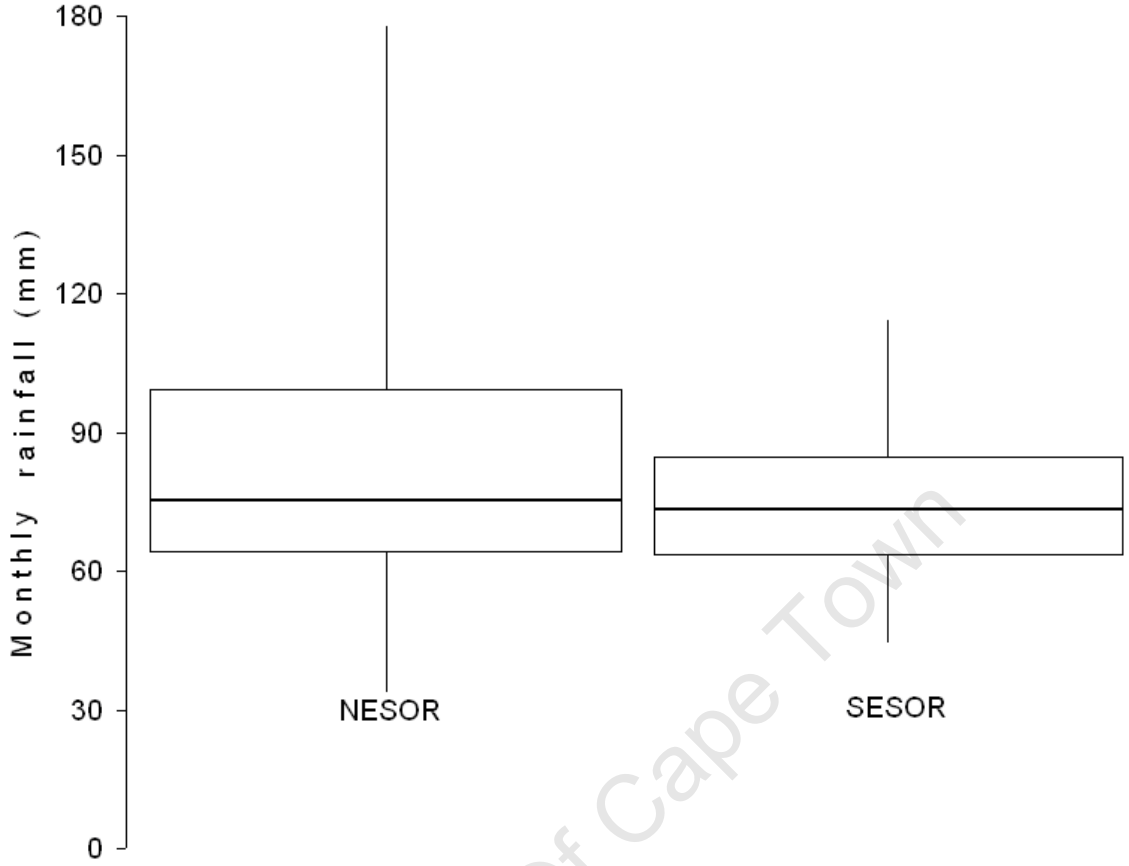

Figure 4.4. Box plots to compare linear descriptions of NESOR *and S*ESOR *rainfall.*

The long term changes in the two series are examined with the Man Kendall rank statistic ***τ*.** The *τ* values for both NESOR and SESOR are well below the significant $\tau_{0.05}$ at 95% confidence level meaning that no significant long term trends are detected (e.g. Richard et al., 2001). Thus although the bar graphs depicting interannual rainfall variability for NESOR and SESOR (not shown) indicate that there are year to year random fluctuations, there appear to be no systematic climate change trend in any of these series. However, the negative estimate of τ for SESOR implies a declining tendency while a positive sign for NESOR indicates an inclination towards escalation.

We further compared the short-term persistent wet and dry periods of the two rainfall series by applying Cramer's t-test for 31 year running means. This statistic compares the means for the sub periods with the mean of the whole period. However, here the statistic has been used to isolate only periods of surplus and deficit rainfall but ignored to examine their significance. A similar approach was adopted by Kripalani and Kulkarni (2001) and Kruger (1999), on Indian monsoon and South African rainfall respectively. The temporal evolution of the 31-year Cramer's t-test is presented in figure 4.5.

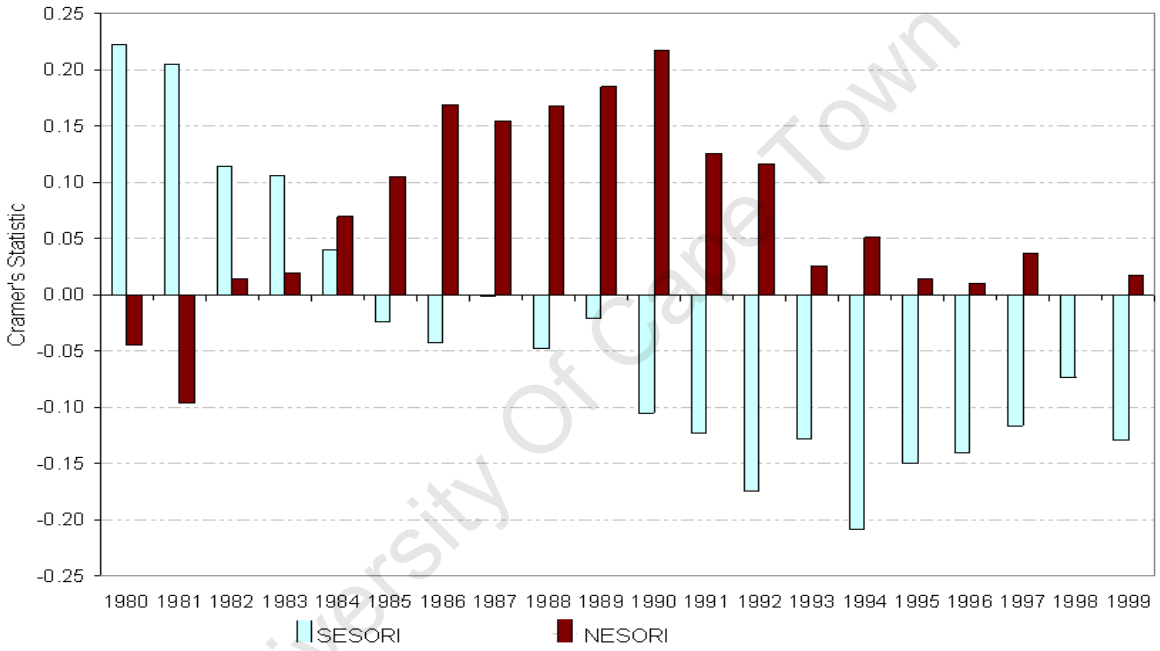

Figure 4.5 Comparison of values of the Cramer's t statistic for the 31 year running means of NESOR and SESOR OND rainfall depicting their decadal variability. The values are at the end of the 31- year segment

There is a high inverse relationship between NESOR and SESOR indexes on interannual time scales, indicating that the periods of high NESOR activity co-occurred with years of subdued SESOR activity, with an interval of about 16 years. Actually there seems to be a systematic pattern being followed by the t-statistic within these opposing

epochs. For example, there is a conspicuous 4 year time lag in these epochal relationships. Consequently, in the oppositely signed individual years of the two rainfall series, the t-statistic with relatively high amplitude mostly coincides with subdued activity. Thus the turning point for SESOR's negative epoch (1984) comes in the forth year after the NESOR's negative epoch had reversed sign (1981), so are the maximum and minimum t statistic for the former (1994) and the latter (1990). Since these two extreme values are located near the center of the respective epochs, it implies that the turning point in the decadal rainfall activity is halfway through each epoch. This clearly depicts the existence of an inverse interplay between NESOR and SESOR regimes on interannual and decadal time scales. These variations are characterized by shifting epochal regimes with defined 4 year time lags. However, if this behavior is able to reflect in the longer time series, then it could serve as a guiding tool in long term predictions of the OND rainfall over the two coherent regions. This aspect needs some explanations and hence we turn to the dominant ocean atmosphere coupled modes located in the tropical Indian Ocean and Pacific Ocean for possible indicators.

4.4 Relation of NESORI and SESORI with the Indo-Pacific SSTs

To demonstrate how the NESOR and SESOR are linked to the dominant tropical SST modes located in the Pacific Ocean and adjacent Indian Ocean, we correlated these indices to the basin wide concurrent SSTs of the two oceans for the period 1950 to 1999. The OND period is chosen as it is the period when both ENSO and IODZM events display their common and easily identifiable existence in their respective oceans (Manatsa et al., 2008). Figure 4.6a and b show the respective spatial correlation structure of NESOR and SESOR with SST anomalies in the Indo-Pacific basin.

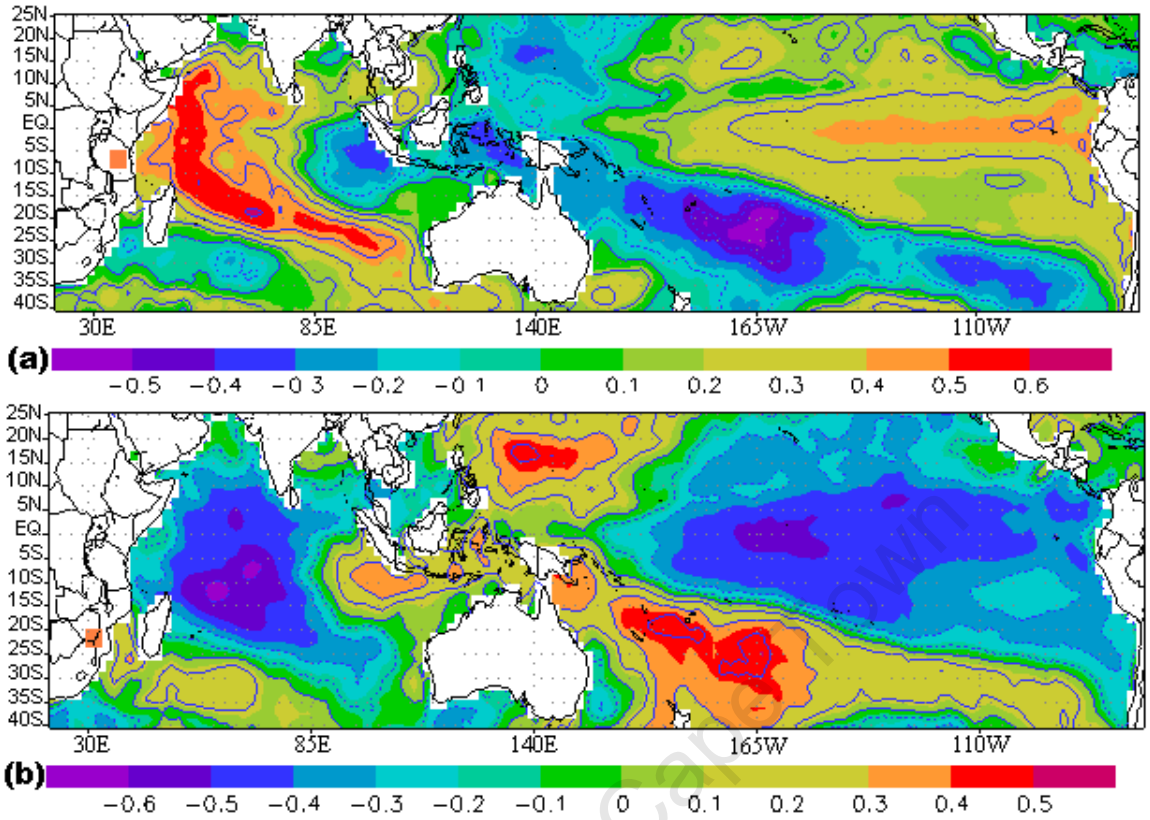

Figure 4.6. The concurrent spatial correlation of (a) NESORI and (b) SESORI with the Indian and Pacific Ocean OND SST anomalies for the period 1950 to 1999. Overland boxes indicate the two areas where the gridded rainfall time series were obtained for NESORI and SESORI. Values above/below +/-0.27(+/-0.37) are significant at 95% (99%) confidence level from as 2 tailed Student's t-test.

It is noteworthy that these correlations are not haphazard, but exhibit rather well defined spatial structures with significant correlation coefficients (above 99% confidence level) that represent the canonical IODZM and ENSO SST anomaly patterns. However the presence of these significant and oppositely signed but similar correlation coefficients patterns for NESOR and SESOR in the Indo-Pacific basin seem to stress that these rainfall anomalies are not only inversely related but strongly connected to large scale atmosphere-ocean coupling. Similar correlation structures to figure 4.6a and b, were

obtained by Behera et al. (2005) and Manatsa et al. (2008), when they studied the connection of the OND rainfall (short rains) and Zimbabwe summer rainfall respectively, with the SSTs in the Indo-Pacific basin. In both cases, relatively high correlation values are found in the tropical Indian Ocean, with the highest values in the western part of the basin. In contrast, the SST anomalies in the tropical Pacific Ocean seem not to be as strongly linked to both NESOR and SESOR. In any case, this observation gives an impression that the two rainfall regimes in the eastern SADC are significantly linked to both ENSO and IODZM. This impression is a false attribution that we will shed light on in the following sections.

On the other hand, in order to study the oppositely signed rainfall variability of these two coherent regions by determining the years in which the magnitude of the dipole pattern was strong, a new rainfall index was formed. This new index is defined simply as NESORI minus SESORI. By so doing these two time series were able to contribute equally to the new index, instead of finding the difference of the actual monthly rainfall anomalies (e.g. Nicholson and Webster, 2007). While this index is not strictly interpretable in terms of the sign of the rainfall anomaly of the region, it does indicate the years when the rainfall disparity between the two regions was relatively large. However, it is prudent to illustrate whether the new time series still preserves the major properties contained in the original NESORI and SESORI. Thus, we correlated the two indices with the newly derived rainfall index. We found the correlation values of +0.85 and -0.87 respectively, which are significant above the 99.99% confidence levels. We also determined the new indices' spatial link to the Indo-Pacific SST basin wide SSTs anomalies by way of cross correlation. Here we note that the previous correlation patterns as depicted in figure 4.6a and b are not only strongly retained, but have acquired higher spatial IODZM and ENSO signals, particularly in the former. Thus we

refer to this new index as, East SADC Meridional Dipole Rainfall Index (ESMDRI), so as to capture the north-south orientation of the 'dipole like' rainfall anomalies.

Combining two indices to enhance a common signal is not new here, but has been done successfully in previous research (e.g. Clark et al., 2003; Jury et al., 2002). So as to see if ESMDRI represents reasonably well the variances explained by ENSO and IODZM phases in the original rainfall series, we considered the explained variances as per the year combinations shown in table 1. The results are shown in Table 3. Here we note that the warm phases of the both IODZM and ENSO phases, especially of the former, explain a considerably greater percentage variance of their respective time series. The same scenario is translated into the three rainfall time series where the pIODZM events explain the greatest variances, followed by El Niño, then nIODZM and lastly La Niña. But however, of particular interest in this analysis is the fact that most explained variances are essentially located between the values explained in NESOR and SESOR. This means that the ESMDRI is able to represent the variability of both time series reasonably well. Thus we are convinced that the above procedure has been able to distil the important properties. The word dipole may be controversial in this context but we retain its use because it has become standard in literature dealing with African rainfall variability. At the same time, it obviously facilitates discussion (e.g. Nicholson and Webster, 2007). Henceforth, the ESMDRI is assumed to adequately represent the temporal manifestation of the opposition in rainfall anomalies signal for the east SADC region and figures 4.13 display its characteristic time evolution from 1950 to 1999.

Table 4.3: *Percentage variance due to all ENSO and IODZM years shown in table 1 for the ENSO, IODZM and ESMDR time series from 1950 to 1999.*

Event SST Phase	Number of Events	Niño 3.4	IODZMI	NESORI	SESORI	ESMDRI
nIODZM	12	10%	29%	15%	1%	2%
pIODZM	12	30%	53%	63%	27%	48%
El Niño	13	60%	35%	23%	16%	19%
La Niña	17	38%	6%	24%	3%	11%

4.5 Spatial Influence of ENSO/IODZMI on SADC OND Rainfall

As noted before, the opposition in rainfall over the northern and southern regions of the eastern SADC has been captured only in the dominant principal component (PC1). It is then logical to expect the mode which has the dominant impact on this region not to miss a similar dipole pattern through correlation analysis. In the bid to prove this hypothesis, we first show the spatial ENSO influence over the SADC region disregarding the influence of IODZM by working out the total correlations as was the case with previous research prior to the discovery of IODZM (e.g. Matarira, 1990). We then do the same with the effect of IODZMI on rainfall, but assuming no interference from ENSO. But by later acknowledging that the signals from the two climate modes do in fact contaminate each other (Ashok et al., 2004) we then employed the partial correlation technique in order to segregate the approximate individual impacts of these phenomena on NESOR/SESOR. Here it has to be noted that Kripalani et al. (2005) displayed discomfort with the application of these techniques to remove the influence of other phenomenon such as this method (to statistically suppress ENSO/IODZM impacts), as they understand that in the real atmosphere IODZM, ENSO and the (east SADC) rainfall are

a part of very large coupled process and are not expected to behave in isolation. In contrast we believe that a partial correlation method is a useful approach to assess independent ENSO/IODZM impacts on the sub region. Moreover, this method has been employed in several works for the same purpose (e.g. Behera et al., 2005; Yamagata et al., 2004; Saji and Yamagata 2003). Thus in a similar manner we also removed the rainfall patterns predictable from the contemporaneous ENSO (IODZM) influence on the correlation between rainfall and the IODZM (ENSO) SSTs in a statistical sense.

Consistent with previous research, figure 4.7(a) shows spatially coherent dipole like patterns of significant (above the 95% confidence level) correlations between ENSO and OND rainfall of eastern SADC. In the northeast SADC region, the correlation is strongest over Tanzania with a value greater than +0.4, whilst it reverses sign over southern SADC where it peaks with a negative correlation value greater than 0.4 magnitude over central and northeast South Africa and, southern Zimbabwe/Mozambique. This status gives an impression that ENSO significantly influences ESMDRI variability, with opposite impacts over the northeast and southern SADC region. Interestingly however, by partialling out the effects due to IODZMI, we see that the area of significant independent ENSO influence shrinks considerably (figure 4.7b). The previous easily identifiable dipole like structure of significant correlations is eliminated almost completely in the process, leaving essentially a monopole mainly over Namibia and southern South Africa. In fact, there is very little or negligible trace of ENSO influence over the eastern SADC region. It becomes quite clear that the ENSO forcing has very little or nothing to do with the oppositely signed correlation pattern. Hence it can be suggested that this structure depicted in figure 4.7a is an apparent effect arising from IODZM events, co-occurring with ENSO. The true ENSO influence over the SADC region is in fact a rather weak inverse monopole rather than a dipole influence. Rather, the importance of the true

ENSO impact regionally can be considered less significant as the influence is relevant mostly in those areas around the south western SADC where rainfall is generally scarce (see figure 4.1).

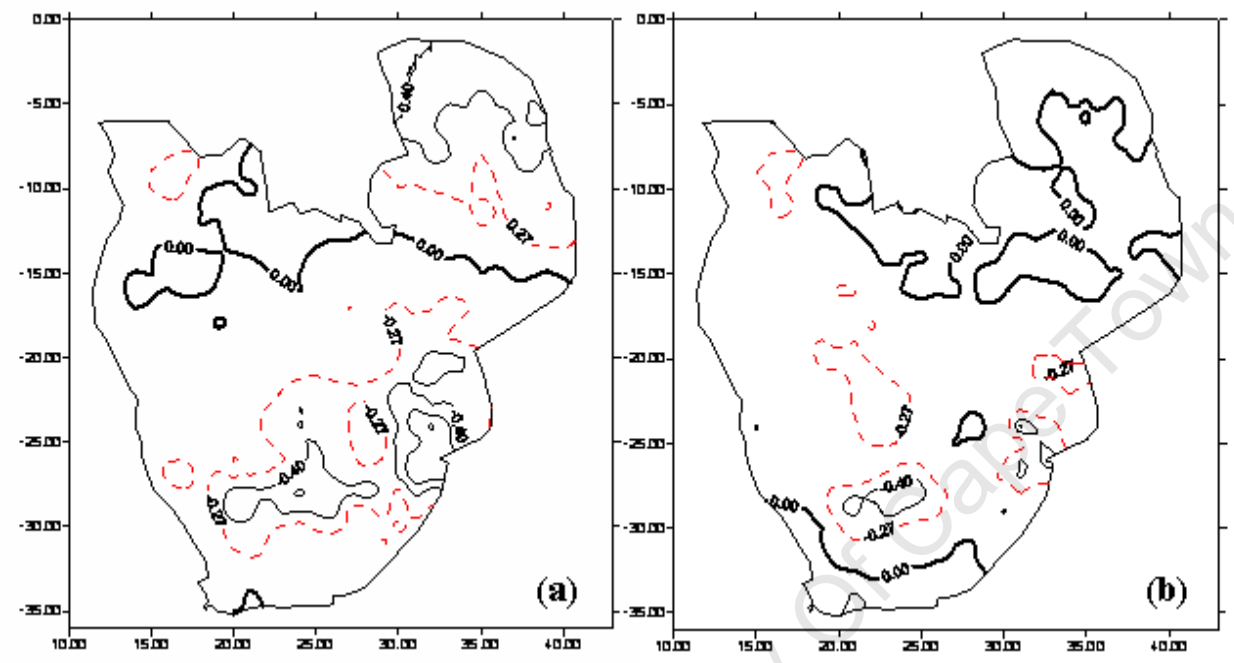

Figure 4.7 Correlation Patterns for SADC OND rainfall (a) with Niño *3.4 SST index and (b) with* Niño *3.4 SST index but when IODZMI is removed (data is from 1951 to 1999). Broken lines show threshold correlation coefficient values that are statistically significant at the 95% confidence levels, using a two-tailed t- test.*

To demonstrate that the IODZM does in fact have a large influence on the opposing rainfall pattern in the eastern SADC region, the IODMI is first correlated to SADC OND rainfall. A spatial pattern similar to that which has been imposed by ENSO is also replicated in the region, except that the correlations are generally stronger especially over Tanzania (figure 4.8a). In a similar fashion, the correlation structure shows values of opposite polarity over the northeast and southeast of the region. However, in order to determine the intrinsic correlation unique only to the IODZM phenomenon (separate from that of ENSO), this general influence is further subjected to the partial correlation technique. The results in figure 4.8b indicate that the opposite polarity pattern with significant correlation values are essentially preserved though both area and strength are reduced over the southeast. Thus in the dipole region of significant influence, the northeast SADC (mostly Tanzania) is undoubtedly the region where the IODZM signal is strongest. The above exercise confirms that a major portion of the interannual variation of the meridional opposition in rainfall over the east SADC region is related to IODZM.

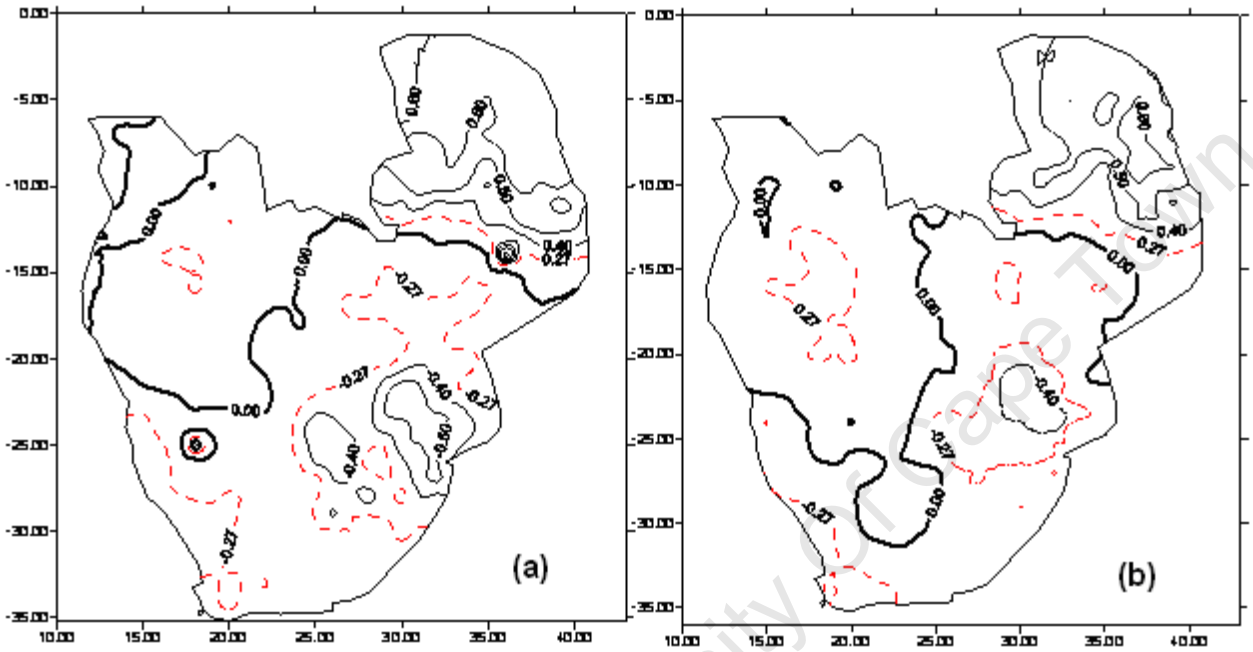

Figure 4.8 Correlation Patterns for SADC OND rainfall (a) with IODZMI and (b) with IODZMI but when ENSO is removed (data is from 1951 to 1999). Broken lines show threshold correlation coefficient values of ±0.27 that are statistically significant at the 95% confidence levels, using a two-tailed t- test.

4.6 Composite Analysis of ENSO and IODZM events on SADC OND rainfall

In order to clarify further on our observation of the IODZM's paramount control of the meridional opposition in rainfall anomalies over the east SADC region, we adopted the pure composite technique as used by Ashok et al. (2004). The pure and co-occurrence years forming the composites are derived from Table 1. This method of analysis may provide the opportunity to approximate the true nature of ENSO and IODZM individual and combined influences on rainfall.

Figure 4.9(a) presents a composite of the rainfall anomaly distribution associated with all the El Niño years (pure El Niño + co-occurrence events), from 1950 to 1999. In this figure, we note that the patterns of significant rainfall anomalies clearly depict a dipole pattern with positive and negative anomalies over the northeast and southeast respectively. Consistent with earlier analysis, no dipole pattern can be easily noted in figure 4.9b, which is a composite of pure El Niño years. The pockets of significant anomalies do not show any coherent patterns and neither do they even suggest a dipole pattern in the remotest sense. This may imply that the years of co-occurrence, which have been removed from figure 4.9a, were mostly responsible for the dipole pattern. Thus it could be concluded that the influence of El Niño events on the subregion may have been overrated, especially as the prime cause of this meridionally aligned opposition in rainfall anomalies over the east SADC.

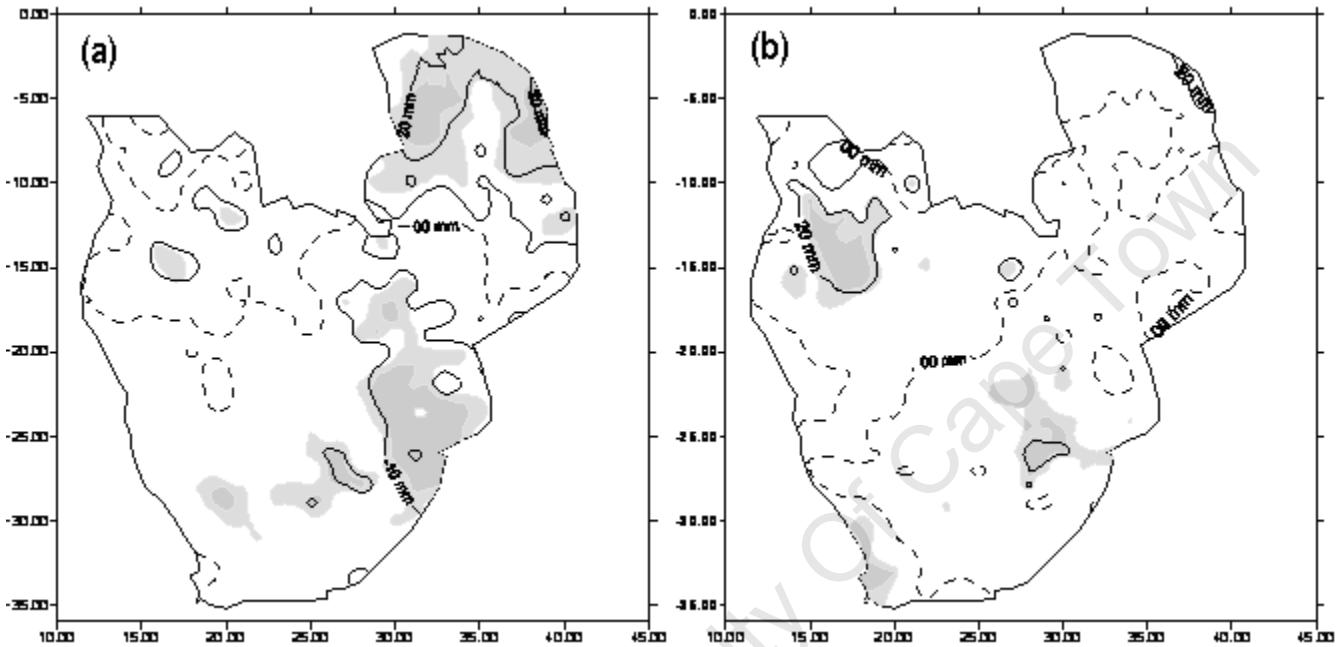

Figure 4.9 Composite of SADC OND monthly mean rainfall (mm) for (a) all El Niño *(El* Niño + *positive IODZM) years (b) pure El* Niño *years for the period 1950 to 1999. Lighter and darker shading represent regions of statistical significance above the 90% and 95% confidence intervals using a 2 tailed t-test.*

A similar investigation is done but using the warm phase composites of IODZM events. The spatial structure resulting from the influence of all positive IODZM events (pure positive IODZM events + co-occurrence events), is presented in figure 4.10 (a). Coherent wet conditions are restricted to the northeastern region while relatively dry conditions prevail over the southeast. We also note an area of significant rainfall anomalies over the central northwestern areas but with the same sign as the northeast. Here it has to be noted that the limited number (3) of events constituting the pure pIODZM composite may actually limit the confidence in the interpretation of this sample (figure 4.10b). However, it can still be easily observed that there is a significant retention of the opposition in rainfall anomaly signature over the eastern region when the IODZM impact is refined to include only these pure positive IODZM events. The difference though minor, is that both magnitude and area of significant deficits over the southeast, are considerably reduced. Thus the independent pIODZM occurrences, rather than pure El Niño events are able to build up significant rainfall enhancement mechanisms over the northeast SADC while at the same time significantly suppressing these mechanisms over the southeast.

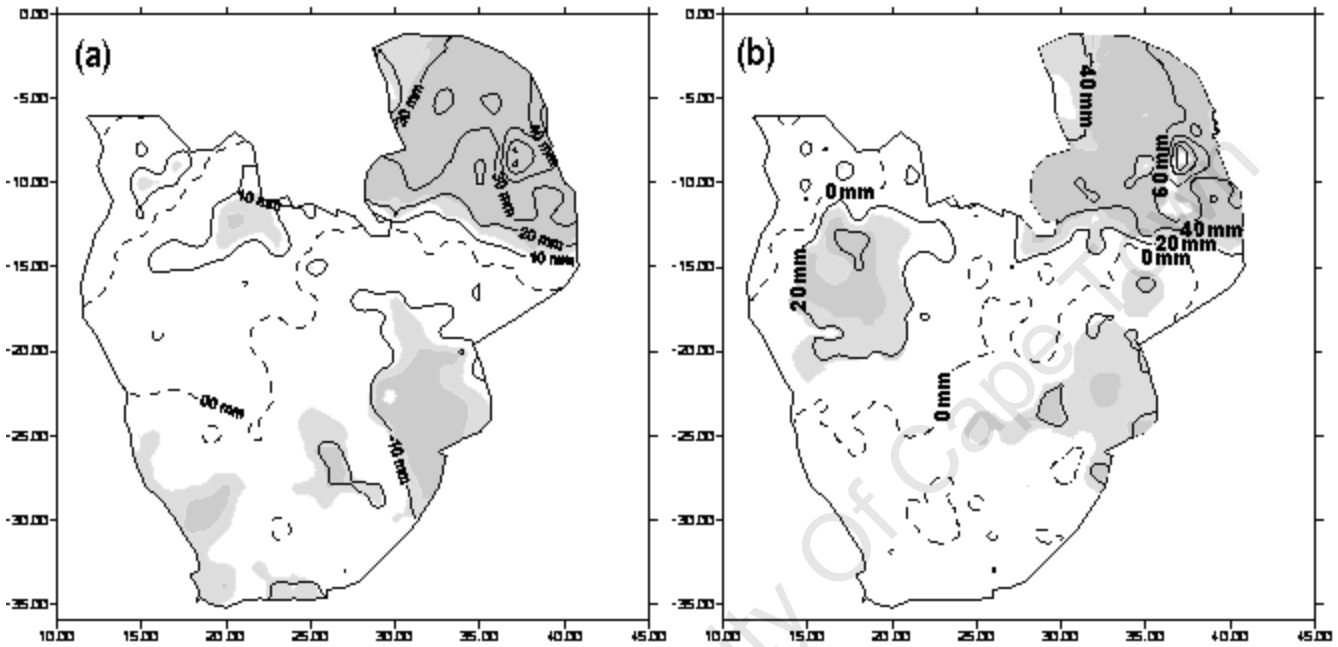

Figure 4.10 Composite of SADC OND rainfall (mm) for (a) all positive IODZM years (b) pure positive IODZM years for the period 1950 to 1999. Lighter and darker shading represent regions of statistical significance above the 90% and 95% confidence intervals using a 2 tailed t-test.

Consideration of the relative effects of the cold phases of these two phenomena is equally important. This is because studying both the warm and cold phase impacts on rainfall assists in avoiding the tempting assumption of symmetry in ENSO/IODZM phase impacts. This has not been verified in other research (e.g. Black et al., 2003, Clark et al., 2003). Figure 4.11 (a) depicts the composite OND rainfall anomaly distribution during all the La Niña years. A dipole pattern in rainfall anomalies is visible but not as coherent as in the previous composites for pIODZM events. But by removing the co-occurring years (figure 4.11b), the dipole pattern is weakened substantially. It thus seems as if this process has also effectively eliminated the opposing rainfall anomaly pattern as the dipole signature becomes considerably ill defined. Surprisingly, although pure La Niña seems unable to generate the dipole pattern, it seems it is able to generate significant positive anomalies over the southern areas. This shows some degree of asymmetry in the ENSO phase impacts. Pure El Niño and pure La Niña seem to induce asymmetric impacts over the SADC region. Similar analysis of all the nIODZM and pure nIODZM composites yielded relatively weak dipole structures as compared to their positive counterparts (not shown). However the dipole influence is even weaker in both magnitude and area for the pure nIODZM composites. Thus the nIODZM events may be interpreted as possibly inheriting the reverse but considerably reduced influence relative to pIODZM on the subregion.

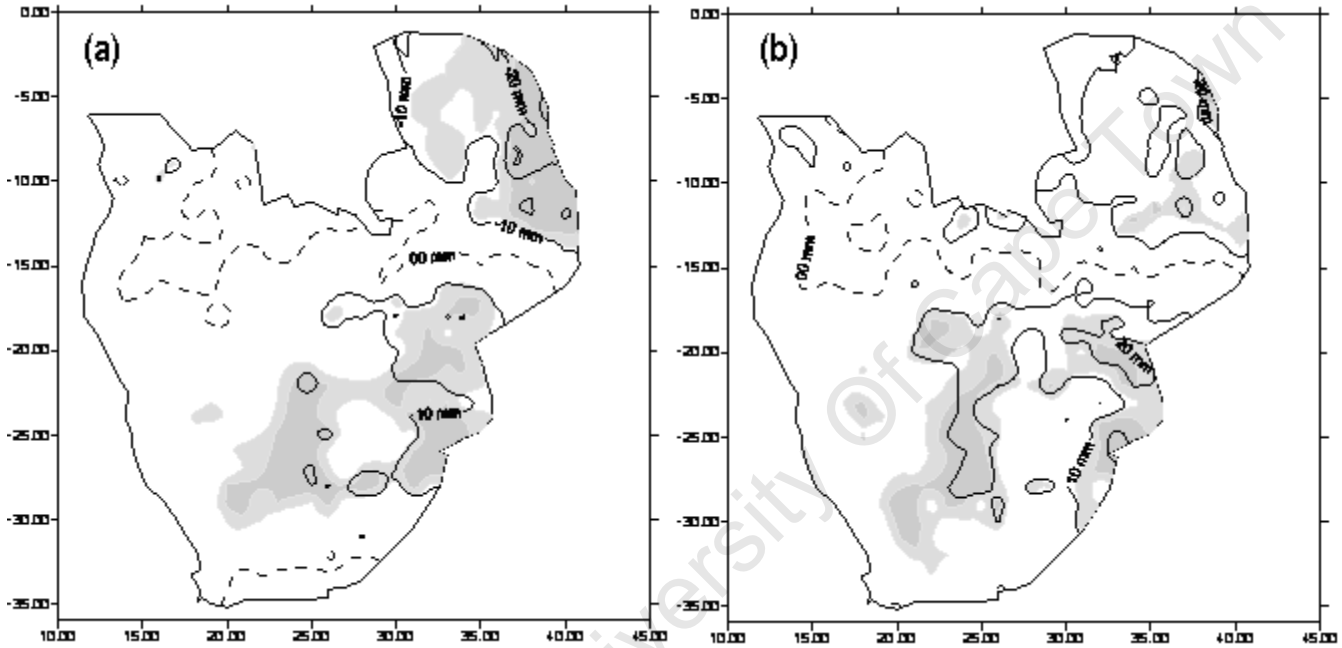

Figure 4.11 Composite of SADC OND monthly rainfall (mm) for (a) all La Niña *years (b) pure La* Niña *years for the period 1950 to 1999. Lighter and darker shading represent regions of statistical significance above the 90% and 95% confidence intervals using a 2 tailed t-test.*

Finally since we removed the co-occurrence years from all their respective events, to come up with a typical uncontaminated event composite, it could be interesting to investigate the nature of their impacts on the rainfall. We see in figure 4.12 (a) and (b) that the opposition in the rainfall regime over eastern SADC is clearly defined in the warm concurrent ENSO and IODZM events (figure 4.12a) but weakly defined in the simultaneous cold events (figure 4.12b). In the absence of the knowledge of IODZM phenomenon these coexisting influences could have been mistaken as the sole impact of the ENSO phases (e.g. Jury et al., 2002; Nicholson and Kim 1997). However we note that the spatial structure of the anomaly composites of the concurrent warm events is considerably more robust than the composites defined by pure IODZM events. This may imply that the dipole structure could be more developed in years of concurrent warm events than in the pure pIODZM events. Even though, it still remains that the well documented oppositely signed rainfall anomalies over the eastern SADC region could be dominantly controlled by the tropical Indian Ocean rather than by the eastern Pacific. However, on the overall, these results may provide preliminary but ample evidence that El Niño produces the anticipated rainfall response in the eastern SADC only when it coincides with a pIODZM event. This strongly supports the conclusion that the warm IODZM events exert a critical influence on rainfall variability over eastern SADC and that the well-documented rainfall link to El Niño is not only highly amplified, but largely a manifestation of co-occurring warm IODZM influence.

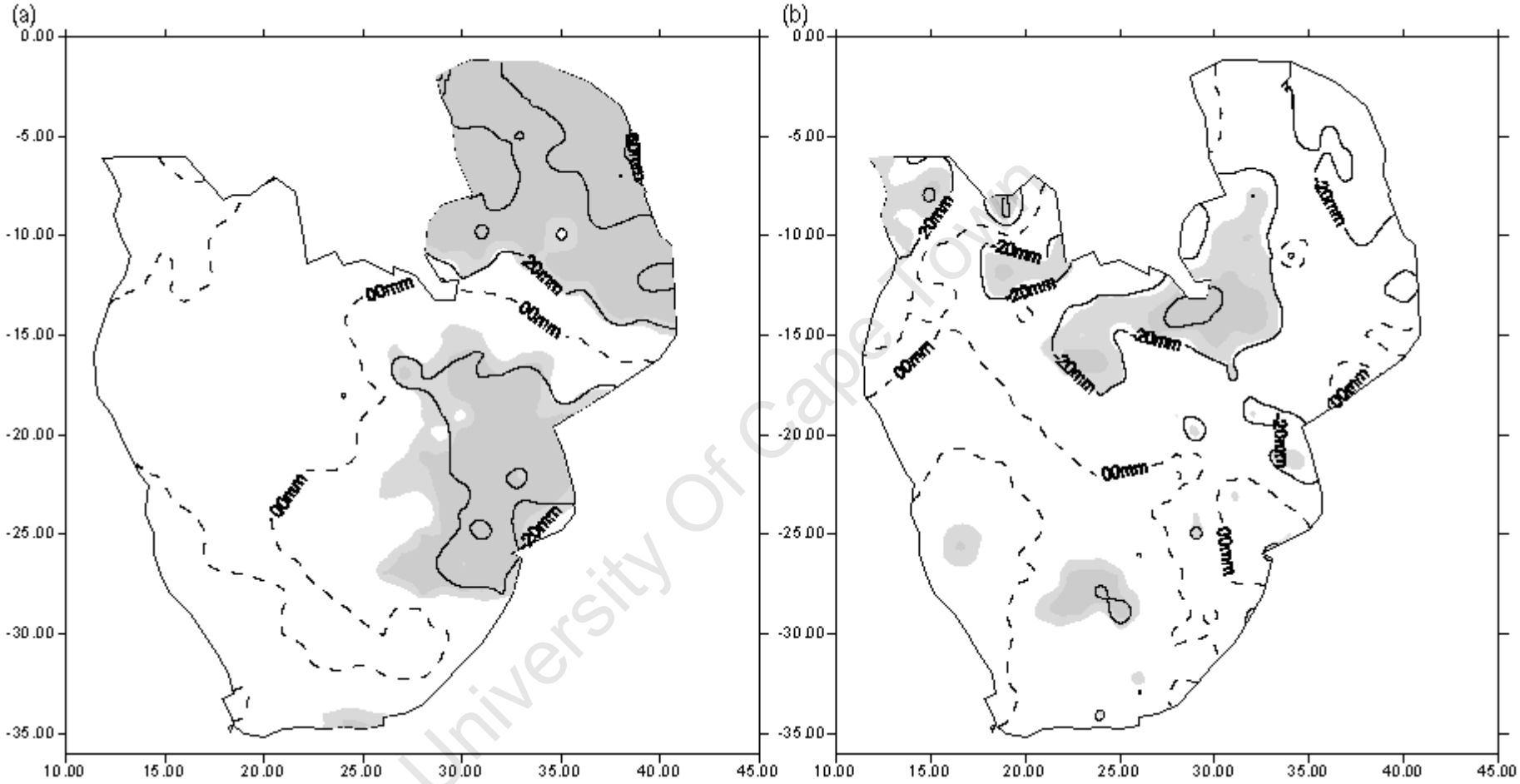

Figure 4.12 Composite of SADC OND monthly rainfall (mm) for (a) Co-occurrence of pIODZM and El Niño *years (b) La* Niña *and negative IODZM years for the period 1950 to 1999. Lighter and darker shading represent regions of statistical significance above the 90% and 95% confidence intervals using a 2 tailed t-test.*

4.7 Temporal Evolution of the impacts of ENSO and/or IODZMI on ESMDRI

This work would be inadequate if the temporal variations of linkages in the time series are not taken into account. It is essential to document the degree of stationarity in these relationships because in many regional applications involving ENSO, stationarity is assumed. In the process of scrutinizing the stability/instability of these associations, insights into the evaluation of the past and future performance of the current ENSO based regional seasonal forecasting schemes can be determined. In addition, doing a temporal comparative analysis involving the IODZM also provides the true value of the new Indian Ocean tropically based climate mode. We have noted that its positive phase is already proving to be a strong potential candidate that can compete fairly well with ENSO as the principal east SADC OND rainfall predictor. However, this is essentially based on our earlier assumptions that ignored temporal variations yet it is quite possible that the validity of certain potential predictors may experience significant interdecadal variations (Kumar et al., 1999). This may lead to a point that although (no) significant relation exists between ENSO/IODZM and the dipole early summer precipitation patterns over east SADC, it is possible that this relationship is quite (in) significant during some period, and this relationship may be (strengthened) weakened or even reversed during other periods, which results in an (significant) insignificant correlation for the total data period. Hence the previous correlation values that have been calculated using the entire period from 1950 to 1999 could be misleading and leave us under the delusion that these correlations are final and hence temporarily stable. Therefore in order to check this possibility, in this section we consider the temporal stability of the relationships by employing a 31 year sliding correlation technique in both simple and partial forms (Kumar et al., 1999).

To illustrate how the see-saw variations in rainfall of the eastern SADC region is temporarily related to ENSO and IODZM, we calculated the sliding correlations of the two climate modes and ESMDRI for the period 1950 to 1999 (figure 4.13). We superimposed in this figure, the running correlation graph between NESORI and SESORI, which is reversed in sign to ease comparison. It is quite clear that these temporal connections are not stable though are significant above the 95% confidence level throughout. However the relationship of ESMDRI and IODZMI is stronger and seem to exhibit a temporal pattern that is similar to the time evolution of the correlation between NESORI and SESORI. This may give us a clue on the closer association of IODZMI to the rainfall than of ENSO to the same.

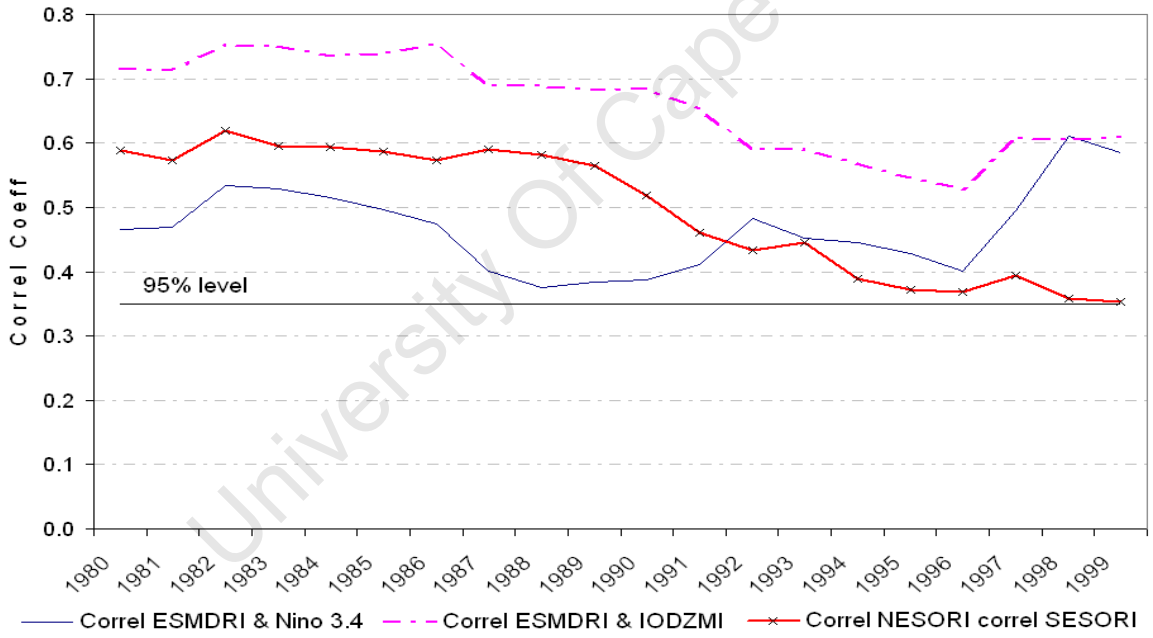

Figure 4.13 Temporal evolution of the 31-year sliding correlation coefficients between ESMDRI and IODMI (broken line) along with that of ESMDRI and Niño *3.4 (solid line). The time manifestation of the running correlation coefficients between NESOR and SESOR is inserted (continuous line with crosses) but reversed in sign to ease comparison. Years are for the end of the 31-year period. The horizontal solid line indicates the 95% significant level.*

The above description suits a scenario in which ENSO and IODZMI do not interact at times. But because of the known interrelationship, we applied the partial correlation method so as to segregate the supposed true ENSO and IODZMI impact on the rainfall. It is the temporal manifestation of these independent correlations in figure 4.14 that confirms our earlier regional predictor instability fears. We note that there are apparent complementary interdecadal changes between the ENSO–ESMDRI and IODZM–ESMDRI relationships especially after about 1986. There is a near mirror image, in the independent ENSO and IODZMI influence of ESMDRI with the years 1990 and 1997 showing notable turning points. This may indicate that IODZM processes which enhance the opposition in rainfall anomalies became closely but inversely related to the ENSO associated processes that suppress the same over the eastern SADC region and vise versa. In other words the effects of independent IODZM on ESMDR varied complementarily with that of ENSO (figure 4.7).

We will not discuss the mechanism that could be responsible for this pattern of relationship between ENSO/IODZM phenomena on the ESMDR rainfall as it is beyond the scope of this work. However, it is quite interesting that the IODZMI independent influence has been gradually losing its linear connection with ESMDRI from the 1990s and ultimately lost the significant link after 1997. At the same time that of ENSO has been gaining in strength. This gradual disconnection (connection) of IODZM (ENSO) and eventually the reversal of the relationships after 1998 is quite essential as the transition made independent ENSO more influential than IODZMI. This is unprecedented and suggests that the eastern SADC sector exhibits a rather unstable and/or non linear ENSO/IODZM related anomaly signal. The transformation to independent ENSO dominance after 1997 is also supported by Manatsa et al. (2009), who analysed the SST data from 1900 to 2006 but used Zimbabwe rainfall data. Therefore, the pronouncement

by Camberlin et al. (2001) that the 'ENSO forcing is virtually undisputed in the regions bordering the Indian Ocean from equatorial Africa to South Africa', could be accurate, only that it was declared a little bit earlier when independent ENSO impact was relatively very weak.

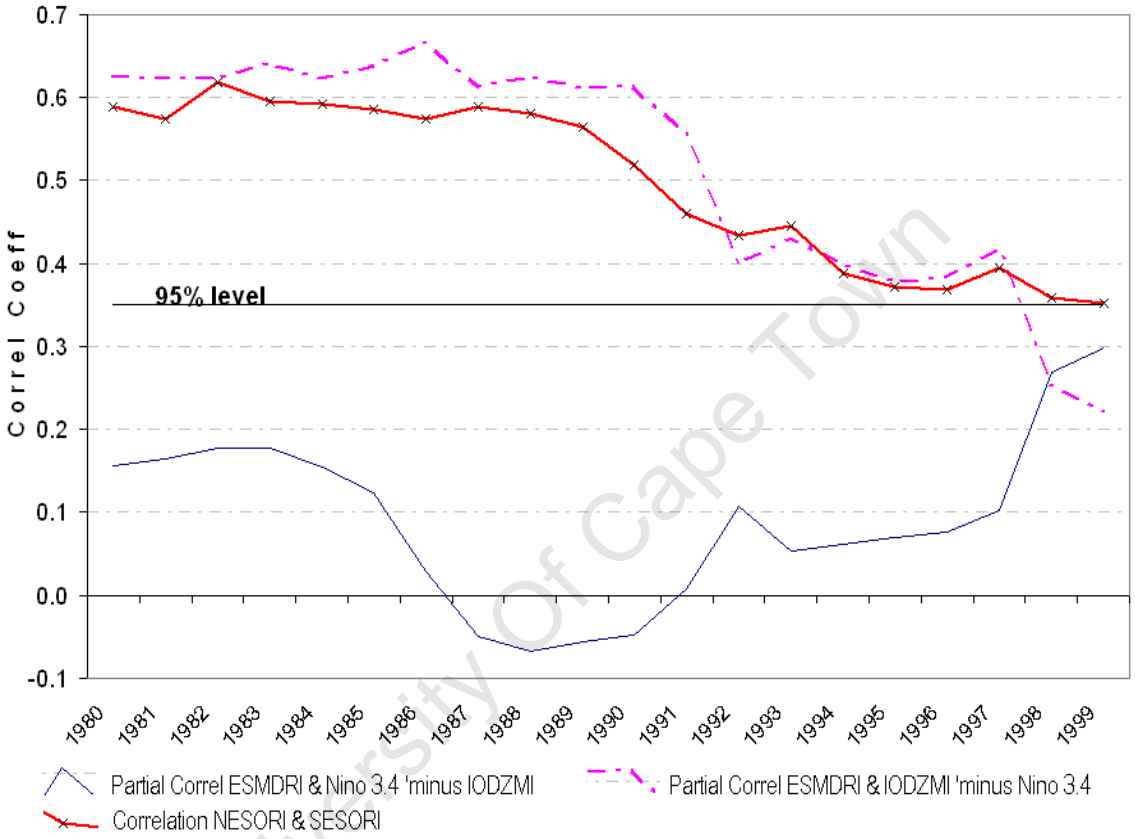

Figure 4.14. Temporal evolution of the 31-year sliding partial correlation coefficients between ESMD rainfall index and IODMI when Niño 3.4 signal is partialed out (broken line) along with that of ESMD rainfall index and Niño *3.4 index when IODZM influence is statistically removed (continuous line). The time manifestation of the running correlation coefficients between NESOR and SESOR is inserted (continuous line with crosses) but reversed in sign to ease comparison. Years are for the end of the 31-year period. The horizontal solid line indicates the 95% significant level.*

4.8 Comparative Wavelet Analysis of ESMDRI, IODZM and Niño 3.4 SST Index

The IODZM has been observed as being the dominant coupled mode influencing the meridional dipole like rainfall anomaly characteristics. We therefore expect the wavelet properties of the IODZM and rainfall indices to display more similarities than with Niño 3.4 SST index. To prove this hypothesis, we employ the wavelet analysis so as to assist in revealing some temporary structures that could have escaped earlier scrutiny in our non stationary time series analysis.

Because in this case we are dealing with finite-length time series, errors will occur at the beginning and end of the wavelet power spectrum, as the Fourier transform method used assumes that the data is cyclic. Thus we opted for the conventional technique to pad the end of the time series with zeroes before doing the wavelet transform and then remove them afterward. This has the effect of limiting the edge effects and speeding up the Fourier transform. But this padding with zeroes introduces discontinuities at the endpoints and decreases the amplitude near the edges as more zeroes enter the analysis. Hence the *cone of influence* is the region of the wavelet spectrum in which edge effects become more important. However, it should be noted that for cyclic series, there is no need to pad with zeroes, and there is no cone of influence. The cone of influence here is indicated in figures 4.15(a) to 4.17(a) by the crosshatched regions. The peaks within these regions have presumably been reduced in magnitude due to the zero padding. Thus, when analyzing, one should be careful as it is unclear whether the decrease in power near the edges is a true decrease in variance or an artifact of the padding.

Results from the global wavelet spectra analysis for Niño 3.4, IODZMI, and ESMDRI and their corresponding global wavelet spectra (GWS) are shown in figure 4.15 (a, b) figure

4.16 (a, b) and figure 4.17 (a, b) respectively. By using significance tests that allow one to verify that interdecadal variance changes in the time series are statistically significant (Torrance and Compo 1998), we note that on the overall, the wavelet power spectra for the three time series show that there is significant (at 10% level) non-stationarity in the variances. This is depicted by black contours demarcating the 90% confidence regions, using the red noise background spectrum.

The power spectrum associated with ESMDR Index reveals that most of the prominent periodic elements of the rainfall variability are observed in the quasi biennial time scales where the significance is at 90% confidence level (figure 4.15). This occurs at two time intervals from about 1959 to 1970 and from 1994 to 1998 but stronger in the latter. The period in between these two intervals from 1950 to 1981, is mostly occupied by another statistically significant periodic element but which operates on decadal time scales. The period displays an arc like curvature of the spectral peak in this wavelet spectra that suggest a continual lengthening of the periodicity of oscillation from the 1950s (16 years) till the mid 1960s (24 years). However, caution has to be taken in the interpretation of this epoch as it lies inside the cone of influence. The peaks within this region have presumably been underrated due to zero padding and it becomes unclear whether the decrease in the band power in this cross hatched region is a true decrease in variance or an artifact of the padding. This leaves the episode from the early 1980s to the mid 1990s as a relatively a quiescent period for the ESMD rainfall. The significance in the periodicities is also confirmed by an integration of power over time figure 4.15 (b) that shows significant power (above the 10% significant level) in the corresponding GWS at the 2 year and 16 to 24 year periodicities, assuming white noise represented by the dashed lines. The latter period is consistent with several studies (e.g. Tyson and Preston-Whyte 2000; Reason and Rouault, 2002; Rouault and Richard, 2005) which

related the epochal variability of southern African rainfall to a quasi-periodic non-random rainfall oscillation with a period of 18 to 20 years. It is interesting to note that this 16 year period was also noted in the SESOR and NESOR 31 year segmented running values of the Cramer's t statistic in figure 4.5.

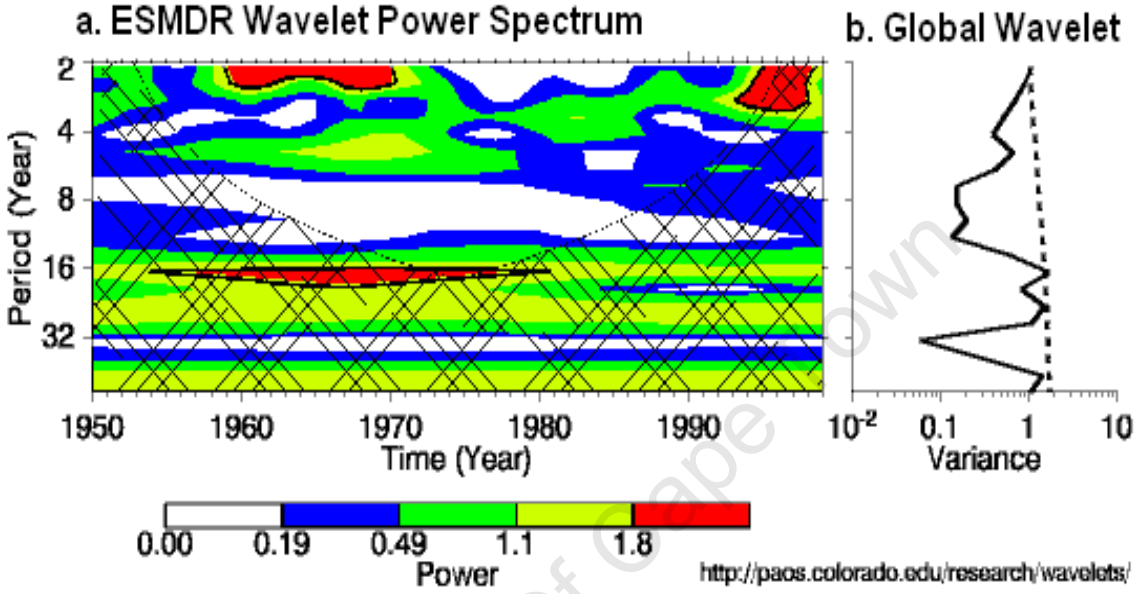

Figure 4.15 (a) ESDMRI wavelet power spectrum with contour levels of 75%, 50%, 25%, and 10% of the wavelet power that are above each level, respectively. The cross-hatched region is the cone of influence, where zero padding has reduced the variance. Black contour is the 10% significance level, using a white-noise background spectrum and (b) is the global wavelet power spectrum (black line). The dashed line is the significance for the global wavelet spectrum, assuming the same significance level and background spectrum as in (a).

In the IODZMI however, the spectrum peaks (figure 4.16a) appear to evolve with the same frequency during adjacent times with ESMDRI especially in the near 2 year band. In this band significant regions of higher variance for both times series coincide in the intervals from 1959 to 1970 and 1994 to 1998. The lengthening of the frequency noted in

the IODZMI was also reflected in the ESMDRI spectrum with the common interval from the early 1960s to the early 1980s. However the corresponding periodicities differ, being 4 to 6 years and 16 to 24 years respectively. Consequently the dormant period for both time series is noted to also coincide at the interval from the mid 1980s to the early 1990s. As with Niño 3.4 (figure 4.17a), the power is mostly concentrated in the 4 to 6 year band where the only significant global wavelet is found. Thus it is to be noted that the significant interdecadal power that characterizes ESMDRI appears not to be present in the Niño 3.4 spectra.

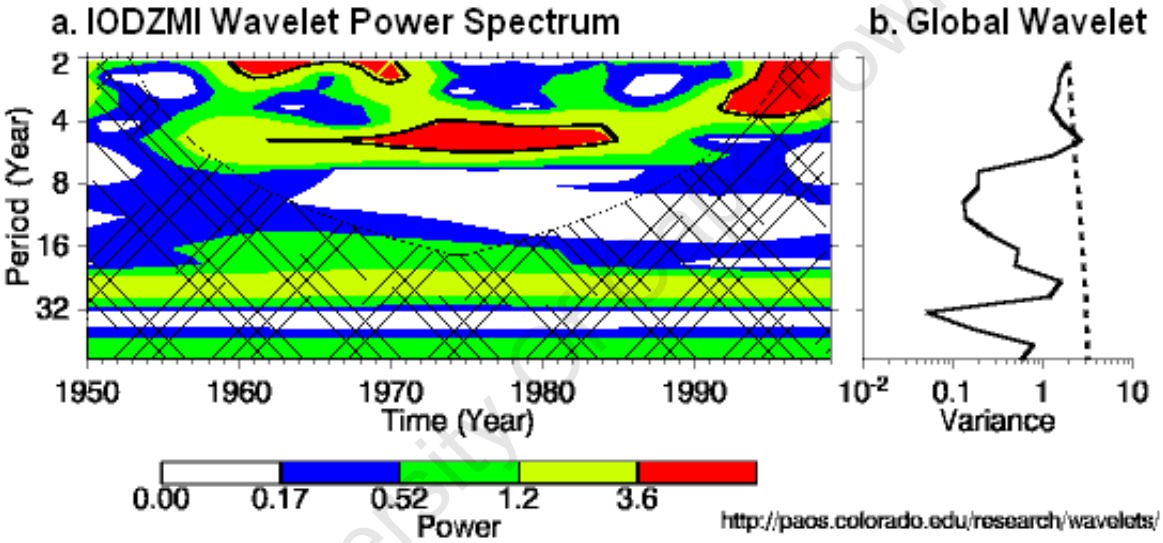

Figure 4.16. Same as in figure 4.15 but for the IODZM SST Index.

On the other hand, the wavelet spectra for IODZMI and Niño 3.4 show significant differences. For example, ENSO activity appears to be weaker during times of high IODZMI variance and *vise versa* (e.g. Saji and Yamagata, 2003). In fact, dissimilarities in the wavelet spectra of Niño 3.4 and IODZMI could be contrasted with the similarities between those of IODZMI and ESMDRI. A typical case, are the intervals from 1950 to 1960 and from 1980 to 1990 where we see ENSO activity at its height. These contrast sharply with IODZMI and ESMDRI as these are the coinciding periods when the activity

of these two time series is quite dormant. Thus, as far as the non stationarity variation is concerned, the time intervals of significant wavelet power spectrum of ESMDRI coincide more with that of IODZMI than with Niño 3.4.

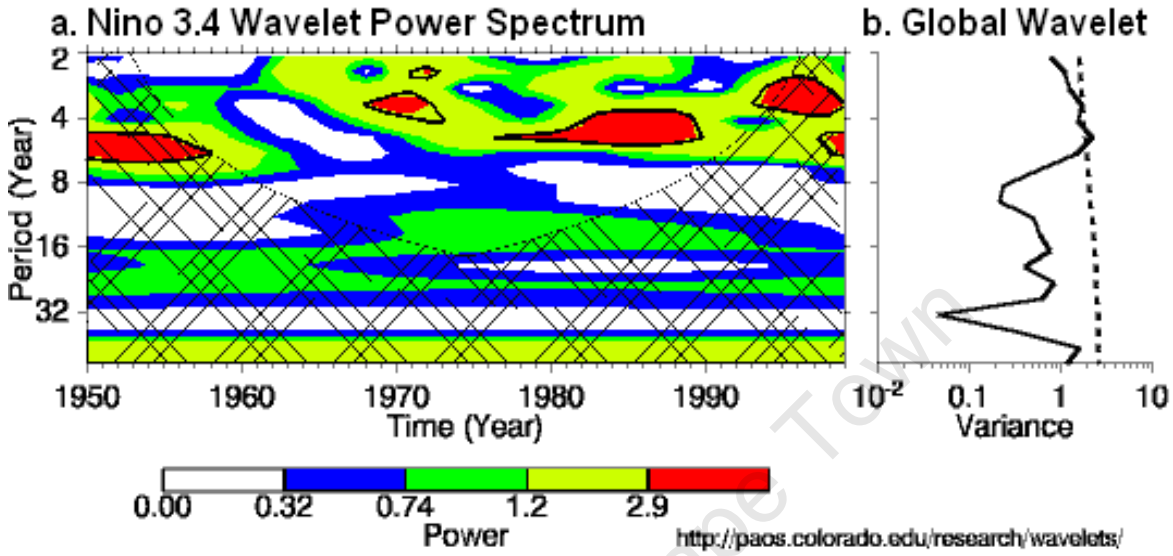

Figure 4.17. Same as in figure 4.15 but for the Niño 3.4 Index.

4.9 ESMDR index amplitude relationship with ENSO and IODZM

Statistical correlation used in earlier sections, only captures the phase relationships between two time series but cannot identify linkages that are not linear. They are also unable to adequately resolve connections that are not temporarily symmetrical. At the same time, the pure composite method that has been used previously obliterates the temporal evolution of the rainfall anomalies within a particular composite. Hence, to bring out a clearer picture on the nature of how ENSO and IODZM phase events influence ESMDR anomalies, it is important to check on the amplitude variations particularly during extreme years. It is the extreme years that underscore the most salient contrasts between the types of events being analysed. Extreme years are easy to identify because one of the most outstanding characteristics of the region depicted in figure 4.18 is that the ESMDRI shows a remarkable degree of spatial coherence as already emphasised

by the earlier EOF analysis. Figure 4.18 also shows that two basic configurations of rainfall anomalies can be easily deduced. The first one (high amplitudes) is the noted meridional dipole with a node around 15°S or 17°S (figure 4.2 a and b) and the second one (low amplitudes) is no dipole years. Since the two patterns have negative and positive phases, the net results are four modes that can also be easily seen in the scatter plot in figure 4.3 for NESORI and SESORI time series. The positive high amplitude meridional dipole mode is when there are generally floods over the northeast and drought over the southeast and its negative mode is when generally, the floods and droughts are reversed in location. The two modes of the low amplitude or no dipole years are when ubiquitous positive or negative anomalies prevail throughout the eastern SADC region.

For brevity we refer to the meridional rainfall dipole event as the year when the ESMDRI magnitude is greater than 0.9. Figures 4.18 (a and b) reveal 9 positive meridional dipole rainfall events above this magnitude and 10 events in the reverse situation. Thus we assigned the ENSO and IODZM phases shown in table 1, to the ESMDRI bar graph. In this way we were able to determine how each individual event is related to the rainfall event amplitude as well as anomaly direction. We first compared the behaviour of pure ENSO events with co-occurrences on the rainfall anomalies (figure 4.18a) before we included the pure IODZM events (figure 4.18b). In figure 4.18(a), we note that, of the 9 warm phase co-occurrence events, 7 coincide with positive ESMDR events of which 6 are meridional rainfall dipole years. However, neither pure El Niño nor pure La Niña displays any plausible link to the meridional dipole rainfall events. The coincidences for these uncontaminated ENSO phases with the dipole years are just too low, 3 out of 10 for La Niña and 1 out of 4 for El Niño. This reflects a very poor linkage between the dipole rainfall patterns and ENSO in its 'pure' form. However, if this association is

reconsidered when the data is not in its entirety, but stratified into *pre and post climate shift* (before and after 1976/77) periods, a new but improved association with La Niña emerges. The entire 6 *pre climate shift* La Niña events coincide with the negative ESMDRI values and better still, 3 of these correspond to meridional dipole events of which two are rated as the strongest. The *post climate shift* era is devoid of any La Niña coexisting with a meridional rainfall dipole event. This suggests that the climate shift could have eroded the once significant link of the La Niña with the ESMDRI. However, the epochal shifts in the relationships are not central in to this study and this will be dealt in subsequent work.

Figure 4.18 (b) is the same as figure 4.18 (a), except that pure ENSO events are replaced with pure IODZM events. However, it is interesting to note that two of the remaining positive meridional rainfall dipole episodes that were left out in figure 4.8a of the pure ENSO analysis (that are also within the highest ESMDRI magnitudes) actually occurred during pure pIODZM events of 1961 and 1967. This factor shows that these independent pIODZM events on their own without the external forcing from the Pacific, can sustain strong positive dipole ESMDR anomalies. Consequently, virtually all but one of the meridional dipole rainfall years is not accounted for by the pIODZM events. Despite this being the case, what is intriguing is that, the ESDMR of 1994 which occurred during one of the strongest pIODZM events of the century (e.g. Annamalai and Murtugude, 2004) is far from being an extreme meridional dipole rainfall event. Even more confusing is that the co-occurrences of 1969 and 1987 seem to have engineered extreme meridional rainfall dipole events but surprisingly, of the unanticipated sign. This reflects the fact that the IODZM-ESDMR relationship is not that straightforward and suggests the existence of other mechanisms suppressing the predictable pIODZM influence during these years.

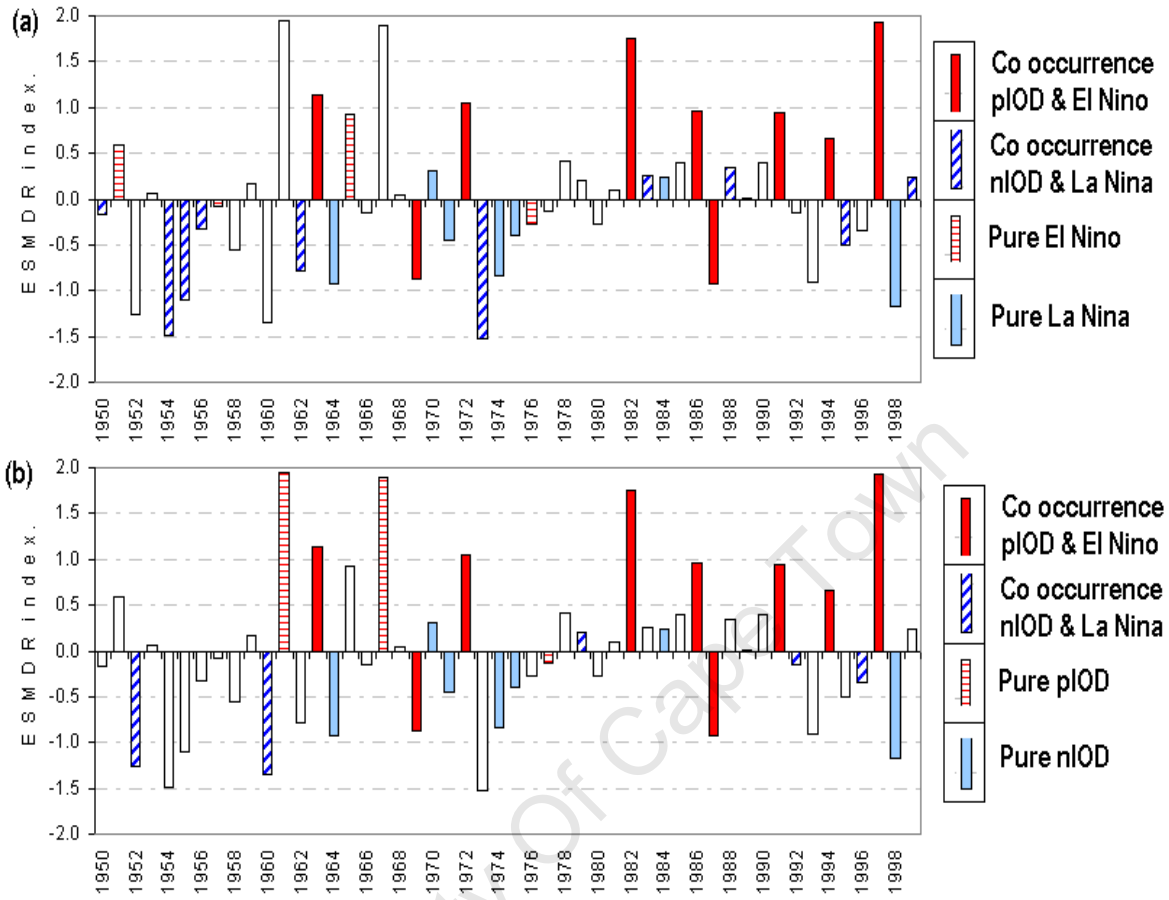

Figure 4.18 ESMDR index (column heights) and their corresponding years with (a) pure ENSO and (b) pure IODZM events with their co-occurrence IODZM and ENSO phase events.

On the other hand the nIODZM events seem to have relatively weak links with the meridional dipole rainfall events should they be pure or in combination with La Niña. Thus the IODZM phase influence is also not symmetrical and the positive phase is the one which is more consistently related to the opposition in rainfall anomalies over the eastern SADC. The connection is such that the excessive rainfall over the northeast is simultaneously accompanied by drought over the southeast of the subregion. As for the reverse situations, when excessive rainfall over the southeast occurs simultaneously

with deficits over the northeast, we see no obvious linear link to both ENSO and nIODZM phases. But there seem to have been some notable linkage with the cold phases of these two climate modes before the climate shift that appear to have vanished after. Therefore it is apparent that the positive and negative extreme ESMDR dipole years have fundamentally different causes. Perhaps other factors such as those emanating from the Atlantic Ocean now dominate the negative phase of extreme ESMDR dipole events (e.g. McHugh and Rogers, 2001; Rouault et al., 2003; Reason et al., 2006). However, it is difficult to deny that nIODZM and/or La Niña was once actively involved in the formulation of negative meridional dipole rainfall events. This is because it is very unlikely that their relatively high coincidences with quite extreme negative ESMDR events that we see in the pre climate shift decades could have occurred by chance. On the other hand, the El Niño seems to have been largely passive throughout the study period in its impacts on the meridional dipole rainfall.

CHAPTER 5:

Discussion and Conclusions

We have used the EOF analysis of OND rainfall over eastern SADC region to illustrate that the northeast and southeast areas are located in different co-variability regions but being captured only in the leading PC. What is also quite apparent here is that the causes of the dipole and non dipole rainfall anomaly patterns are fundamentally different. At the same time, ENSO which is the standard attribute for regional rainfall variability could not adequately explain this dipole rainfall anomaly pattern. Instead there appears to be consistent evidence through statistical techniques employed that strongly link the IODZM events to this opposing rainfall pattern. However, in this novel relationship, it became apparent that the strong positive and negative dipoles of this rainfall pattern have also essentially dissimilar causes. While the pIODZM could be responsible for the positive rainfall dipole, i.e. simultaneous floods over the northeast and droughts over the southeast of the SADC region, the nIODZM is not even remotely linked to the reverse rainfall dipole configuration. Neither is the neutral years related to the non dipole years.

However, we may hypothesise that the meridional displacement of moisture in the regions over east SADC with a node around 16 S is a major factor in the development of the dipole patterns but not in the non dipole patterns. The pIODZM is most probably involved in this meridional displacement of moisture by way of concentrating moisture from the tropical Indian Ocean meant for southern Africa, over east Africa. Jury et al. (2002) has already noted that east African rainfall regime shares the same maritime convection with the tropical Indian Ocean, while convection over southern Africa is inversely related. It is quite clear that the development of opposite process cannot be explained by the nIODZM and that ENSO's linear participation in this process has been

effectively eliminated in this thesis at least in the statistical sense. At the same time these rainfall anomaly dipole years cannot possibly be associated with factors that influence the position of the ITCZ as proposed by Janowiak (1988) because the study period (OND) is such that the ITCZ is not yet quite active over southern Africa (D'Abreton and Tyson, 1995). Therefore, further research is required to investigate the incidence of SST anomalies in the neighbouring oceans especially the Atlantic in the recent decades (e.g. McHugh and Rogers, 2001), that might generate anomalous circulation that could be acting in the maintenance of this meridional dipole structure of rainfall anomalies. This may indicate that in previous works, the widely accepted view that assumed warm ENSO dominant influence has been misconstrued as the prime cause of this meridional dipole rainfall anomaly pattern (Nicholson and Kim, 1997). It has emerged from this thesis, that the role of El Niño could have been largely amplified by the numerous co-occurrences with the pIODZM events.

This observation should not surprise us as other earlier observational and modeling studies (e.g. Nicholson and Kim, 1997; Rocha and Simmonds, 1997; Goddard and Graham 1999; Latif et al., 1999), noted that the ENSO spatial signals over the eastern SADC region were poorly defined. Instead they highlighted the active participation of Indian Ocean SSTs. It is natural to expect that the IODZM, which is located in the prime source of the eastern SADC moisture, has a significant influence on this neighbouring region's rainfall variability. Thus the present analysis therefore demonstrates the power of simple statistical analysis to capture physical climate signals. Most importantly it shows that the results presented here are not artificial outputs of the statistical methods adopted in the study.

Investigating the teleconnections of the OND SADC rainfall has provided insights into the limitations of the current procedure of using ENSO as the primary predictor for the region. First, it has become apparent that there is more widespread significant footprint of IODZM activity, both spatially and temporarily, over the east SADC region than that attributed to ENSO. Despite ENSO being used as the principal predictor by SARCOF in the seasonal forecast over the SADC, there is virtually no detectable evidence to suggest robust ENSO linear influence in this subregion. Secondly, even if we realized that the IODZM influence on eastern SADC region could be paramount; subjecting these relationships to temporal scrutiny using 31 year window widths produced an interesting revelation. We note that both ENSO and IODZMI impact on east SADC region is not temporarily stable and IODZM's once dominant influence has even gradually ceased. Worse still, its force on the rainfall variability has become insignificant towards the end of the 20th century. It then follows that the current method of assuming stationarity in relationships especially when constructing seasonal forecasting schemes could be misleading. Clearly the dynamics governing the relationships between ESMDR and ENSO/IODZM varies inter-decadly. However, better understanding of the causes of these interdecadal variations is needed before improved long lead empirical forecasting of precipitation can be achieved.

Although there is a possibility that some IODZM events could be linked to ENSO processes, the current approach to consider the IODZM as a one of the major coupled modes in the tropics seems to have been successful, at least in evaluating the IODZM's influence on the east SADC region. This finding not only questions the previous notion that the Indian Ocean plays a passive role in the regional climate variability but also gives an indication of the true nature of the ENSO/IODZM regional influence. It provides

new possibilities in advancing the region's rainfall predictability in the sense that in addition to the ENSO, it suggested the existence of an equally comparable coupled mode of variability inherent in the tropical Indian Ocean system. The IODZM has the potential to be used to increase our ability to predict SADC OND rainfall variability on interannual time scales. Consequently, knowledge of the temporal variations of not only ENSO but IODZM is important. This is because these dimensions will dictate the nature (and successful prediction) of interannual rainfall fluctuations over the east SADC region. Also these dimensions will be the best indicator of when and where the ENSO and IODZM teleconnections can be used as reliable predictors of seasonal precipitation.

Lastly, there are a number of questions concerning the causes, dynamical implications and reasons for the above teleconnections which the study has raised and need to be addressed:

- What then is responsible for the negative dipole rainfall events (when drought over the northeast occurs simultaneously with excessive rainfall over the southeast)?
- Why should the decadal variability of SESOR follow that NESOR approximately four years later?
- Why is it that the ENSO influence has gradually became stronger at the expense of the weakening IODZM impacts from the late 1990s?

References

Allan, R., Chambers D, Drosdowsky W, Hendon H, Latif M, Nicholls N, Smith I, Stone R, Tourre Y. 2001. Is there an Indian Ocean Dipole, and is it independent of the El Niño-Southern Oscillation? *CLIVAR Exchanges* **6:** 18-22.

Annamalai H, Murtugudde R. 2004. Role of the Indian Ocean in regional climate variability *Geophysical Monograph* 147**:** 213-246.

Annamalai H, Xie SP, McCreary JP, Murtugudde R. 2004. Impact of the Indian Ocean sea surface temperature on developing El Niño. http://www.soest.hawaii.edu/~hanna/annaetal_jc2004.pdf. Accessed 10/08/2007.

Ashok K, Guan Z, Saji NH, Yamagata T. 2004. Individual and combined influences of ENSO and Indian Ocean Dipole on the Indian Monsoon. *Journal of Climate* **17**: 3141- 3155.

Baquero-Bernal A, and Latif M. 2002. On dipole-like variability in the tropical Indian Ocean. *Journal of Climate* **15:** 11: 1358-1368.

Behera SK, Luo JJ, Masson S, Delecluse P, Gualdi S, Navarra A, and Yamagata T. 2005. Paramount Impact of the Indian Ocean Dipole on the East African Short Rains: A CGCM Study. *Journal of Climate* **18:** 4514-4530.

Behera, S.K. and Yamagata. T., 2003. Influence of the Indian Ocean dipole on the Southern Oscillation. *Journal of Meteorological Society of Japan*, **81, 1**: 169-177.

Buell, C.E. 1975. 'The topography of empirical orthogonal functions', *Preprints Fourth Conference on Probability and Statistics in Atmospheric Science*, Tallahassee, Florida, American Meteorological Society, pp. 188–193.

Black E, Slingo J, Sperber KR. 2003. An observational study of the relationship between excessively strong short rains in coastal east Africa and Indian Ocean SST. *Monthly Weather Review* **131**: 74-94.

Camberlin P, Janicot S, Poccard I. 2001. Seasonality and atmospheric dynamics of the teleconnection between African rainfall and tropical sea-surface temperature: Atlantic vs. ENSO. *International Journal of Climatology* **21**: 973–1005.

Chambers DP, Tapley BD, Stewart RH. 1999. Anomalous warming in the Indian Ocean coincident with El Niño. *Journal of Geophysical Research* **104**: 10523-10533.

Clark CO, Webster PJ, Cole JE. 2003. Interdecadal variability of the relationship between the Indian Ocean zonal mode and East African coastal rainfall anomalies, *Journal of Climate* **16:** 548–554.

D'Abreton PC, Tyson PD. 1995. Divergent and non-divergent water vapour transport over southern Africa during wet and dry conditions. *Meteorology and Atmospheric Phys*ics. **55**: 47-59.

Fauchereau, N, Trazaska S, Rouault M, Richard Y. 2003. Rainfall variability and changes in southern Africa during the last 20th century in the Global Warming context. *Natural Hazards* **29**:139-154.

Goddard L, Graham NE. 1999. The importance of the Indian Ocean for GCM based climate forecasts over eastern and southern interior of Southern Africa. *Journal of Geophysical Research* **104**: 19099-19116.

Hastenrath S., Polzin D., Greischar L. 2002. Annual cycle of equatorial zonal circulation from the ECMWF reanalysis. *Journal of the Meteorological Society of Japan* **80, 4**: 755-766.

Hastenrath S., Polzin D., Camberlin P. 2004. Exploring the predictability of the 'Short Rains' at the coast of east Africa. *International Journal of Climatology* **24**: 1333–1343 DOI:10.1002/joc.1070.

Haylock M. R., P. D. Jones, R. J. Allan, and T. J. Ansell. 2007. Decadal changes in 1870–2004 Northern Hemisphere winter sea level pressure variability and its relationship with surface temperature, *Journal of Geophysical Research*, *112*, D11103, doi: 10.1029/2006JD007291.

Hendon HH. 2003. Indonesian rainfall variability: impacts of ENSO and local air sea interactions. *Journal of Climate* **16**: 1775–1790.

Hotelling, H. 1933. 'Analysis of a complex of statistical variables into principal components'. *Journal of Education Psychology*. **24:** 417-441.

Iizuka S, Matsuura T, Yamagata T, 2000. The Indian Ocean SST Diploe simulated in coupled general circulation model. *Geophysical Research Letter* **27:** 3369-3372.

IMSL. 1987. STAT/LIBRARY, FORTRAN Subroutines for Statistical Analysis. 1232 pp.

Janowiak JE. 1988. An investigation in interannual rainfall variability in Africa. *Journal of Climate* **1**: 240-255.

Jolliffe, I. T., 1986: *Principal Component Analysis.* Springer-Verlag, Berlin, 271 pp.

Jolliffe, I. T., 1987: Rotation of principal components: Some comments. *Journal of Climatology* **7:** 507–510.

Jolliffe, I. T., 1990: Principal component analysis: A beginner's guide. Part I: Introduction and application. *Weather* **45,** 375–382.

Jones P. D. , Hulme M. 1996. Calculating regional climatic time series for temperature and precipitation: Methods and illustrations. *International Journal of Climatology* **16:** 361-377.

Jury MR, Enfield DB, Me´lice J. 2002. Tropical monsoons around Africa: Stability of El Niño–Southern Oscillation associations and links with continental climate. *Journal of Gephysical Research* **107:** 15.1-15.17.

Jury MR. 2002. Economic Impacts of Climate Variability in South Africa and Development of Resource Prediction Models *Journal of Applied Climatology* **41**: 1 46–55.

Jury MR, Mwafulirwa ND. 2002. Climate variability in Malawi, part 1: dry summers, statistical associations and predictability. *International Journal of Climatology* **22**: 1289-1302.

Jury MR, White WB, Reason CJC. 2004. Modeling the dominant climate signals around southern Africa. *Climate Dynamics* **23**: 717–726.

Kaplan A, Cane MA, Kushnir Y, Clement A, Blumenthal M, Rajagopalan B. 1998. Analyses of global sea surface temperature 1856-1991, *Journal of Geophysical Research* **103**, 18,567-18,589.

Kripalani, R.H., Kulkarni A. 2001. Monsoon rainfall variations and teleconnections over south and east Asia. *International Journal of Climatology*. **21**: 603–616.

Kripalani RH, Oh JH, Kang JH, Sabade SS, Kulkarni A (2005) Extreme monsoons over East Asia: Possible role of Indian Ocean Zonal Mode. *Theoretical and Applied Climatology* **82**: 81-94.

Kruger, A.C. 1999. The influence of the decadal scale variability of summer rainfall on the impact of El Niño and La Niña events of South Africa. *International Journal of Climatology* **19**: 59-68.

Kumar KK, Rajagopalan B, Cane MA. 1999. On the weakening relationship between the Indian Monsoon and ENSO. *Science* **284**: 2156-2159 DOI: 10.1126/science. 284.5423.2156.

Latif, M, Dommenget D, Dima M, Grötzner A. 1999. The Role of Indian Ocean Sea Surface Temperature in Forcing East African Rainfall Anomalies during December–January 1997/98. Journal of Climate **12:** 3497–3504.

Legates, D. R., and C. J. Willmott, 1990: Mean seasonal and spatial variability in gauge

corrected global precipitation. *International Journal of. Climatology* **10:** 111–127.

Makarau A., Jury MR, 1997. Predictability of Zimbabwe summer rainfall. *International Journal of Climatology* **17:** 1421–1432.

Manatsa D, Chingombe W, Matsikwa H, Matarira C.H. 2007. The Superior Influence of the Darwin Sea Level pressure anomalies over ENSO as a simple drought predictor for southern Africa. *Theoretical and Applied Climatology* **92:** 1-4. DOI 10.1007/s00704-007-0315-3.

Manatsa D, Chingombe H, Matarira CH. 2008.The Impact of the positive Indian Ocean Dipole on Zimbabwe Droughts. *International Journal of Climatology* **28:** 2011 – 2029. DOI: 10.1002/joc.1695.

Manatsa D, Matarira CH. 2009. Changing dependence of Zimbabwe rainfall variability on ENSO and the Indian Ocean dipole/zonal mode. *Theoretical and Applied Climatology* **98:** 375 – 396. DOI 10.1007/s00704-009-0114-0.

Manatsa D, Matarira CH, Mukwada G. 2009. Relative Impacts of ENSO and Indian Ocean Dipole/zonal mode on east SADC rainfall. *International Journal of Climatology*. DOI: 10.1002/joc.2086.

Manatsa D, Mukwada G, Siziba E, Chinyanganya TP. 2010. Analysis of Multi-Dimensional Aspects of Agricultural Droughts in Zimbabwe using the Standardised Precipitation Index (SPI). *Theoretical and Applied Climatology* DOI: 10.1007/s00704-010-0262-2.

Mapande AT, Reason CJC. 2005. Interannual rainfall variability over Western Tanzania. *International Journal of Climatology* **25***: 1355-1368.*

Marchant R, Mumbi C, Behera S, Yamagata T. 2006. The Indian Ocean Dipole – the unsung driver of climate variability in east Africa. *African Journal of Ecology* **45**: 4-16.

Matarira CH. 1990. Drought over Zimbabwe in a regional and global context. *International Journal of Climatology* **10**: 609–625.

McHugh MJ, Rogers CJ. 2001. North Atlantic Oscillation influence on the precipitation variability around south-east African Convergence Zone. *Journal of Climate* **14***:* 3641-3642.

McHugh MJ. 2006. Impact of south Pacific circulation variability of east African rainfall. *International Journal of Climatology* **26**: 505-521.

Murtugudde R, McCreary Jr JP, Busalacchi AJ. 2000. Oceanic processes associated with anomalous events in the Indian Ocean with relevance to 1997-1998. *Journal of Geophysical Research* **105:** 3295-3306.

Mutai, CC., Ward, MN. 2002. East African Rainfall and the Tropical Circulation/ Convection on Intra-seasonal to Interannual *Timescales. Journal of Climate* **13**: 3915–3939.

Nicholson SE. 2003. Comments on ''The South Indian Convergence Zone and Interannual Rainfall Variability over Southern Africa'' and the Question of ENSO's Influence on Southern Africa. *Journal of Climate* **16:** 555-562.

Nicholson SE, Kim J. 1997. The relationship of El Niño Southern Oscillation to African rainfall. *International Journal of* Climatology **17:** 117-135.

Nicholson S, Webster JP. 2007. A physical basis for the interannual variability of rainfall in the Sahel. *Quarterly Journal of the Royal Meteorological Society* **133**: 2065-2084.

Parthasarathy, K., K., R. Kumar, and A. A. Munot. 1991. Evidence of secular variations in Indian monsoon rainfall-circulation relationships. *Journal of Climate* **4**: 927-938.

Pearson, K.: 1901. On lines and plans of closest fit to systems of points in space. *Philosophical Magazine* **2**: 559-572.

Preston-Whyte, R.A. and Tyson, PD. 1988. *The Atmosphere and Weather of Southern Africa*, Oxford University Press, Cape Town, 374 pp.

Rao, A S., Behera SK, Masumoto Y, Yamagata T. 2002. Interannual subsurface variability in the tropical Indian Ocean with special emphasis on the Indian Ocean dipole. *Deep Sea Research,* **49B:** 1549–1572.

Rayner NA, Horton EB, Parker DE, Folland CK, Hackett RB. 1996. Version 2.2 of the Global Sea-Ice and Sea Surface Temperature Data Set., 1993-1994. Climate Research Technical Note 74 (Hadley Center for Climate Prediction and Research, Meteorological Office, London Road, Bracknell, RG12 2SY).

Reason CJC, Landman W, Tennant W. 2006. Seasonal to decadal prediction of southern African climate and its links with variability of the Atlantic Ocean. *Bulletin of the American Meteorological Society* **87:** 941-955.

Reason CJC, Jagadheesha D. 2005. A model investigation of recent ENSO impacts over southern Africa. *Meteorology and Atmospheric Physics* **89:**181–205.

Reason CJC, Mulenga H. 1999. Relationship between South African Rainfall and SST anomalies in the South West Indian Ocean. *International Journal of Climatology,* **19**: 1651-1763.

Richard Y, Fauchereau N, Poccard I, Rouault M, Trzaska S. 2001. 20th century droughts in southern Africa: spatial and temporal variability, teleconnections with oceanic and atmospheric conditions. *International Journal of* Climatology **21**: 873-885.

Richman, MB. 1986. Rotation of PCs. *International Journal of Climatology* **6:** 293-335.

Rocha A, Simmonds I. 1997. Interannual variability of south-eastern African summer rainfall. Part 1: Relationships with air-sea interaction processes. *International Journal of* Climatology **17**: 235–265.

Rouault M, Florenchie P, Fauchereau N, Reason CJC. 2003. South East Atlantic warm events and southern African rainfall. *Geophysical Research Letters* **30:** 9.1-9.4.

Rouault M, Richard Y. 2005. Intensity and spatial extent of droughts in southern Africa. *Geophysical Research Letters* **32**: L15702, doi:10.1029/2005GL022436.

Ropelewski CF, Halpert MS. 1989. Precipitation patterns associated with the high index phase of the Southern Oscillation. *Journal of Climate* **2**: 268–284.

Saji, NH, Goswami BN, Vinayachandran PN, Yamagata T. 1999. A dipole mode in the tropical Indian Ocean. *Nature* **401**: 360-363.

Saji NH, Yamagata T. 2003. Possible roles of Indian Ocean dipole mode events on global climate. *Climate Research* **25**: 151–169.

Santos CAG, Galvao CO, Suzuki K, Trigo, RM. 2001. Matsuyama city rainfall data analysis using *wavelet* transform. *Journal of Hydraulic Engineering*, JSCE, **45:** 211–216.

Shinoda T., Alexander MA., Hedon HH. 2004. Remote response of the Indian Ocean to interannual SST variations in the Tropical Pacific. *Journal of Climate* **17**: 362–372.

Soman, MK., Slingo, J. 1997. Sensitivity of the Asian summer monsoon to aspects of sea-surface temperature anomalies in the tropical Pacific Ocean. Quarterly Journal of Royal Meteorology Society, **123**: 309-336.

Spiegel, MR. 1988. *Schaum's outline of theory and problems of statistics*, McGraw-Hill, 2nd edition, pp 324-339.

Terry P., Dominiak S., Delecluse P. 2005. Role of the southern Indian Ocean in the transitions of the monsoon-ENSO system during recent decades. Climate Dynamics **24**: 169-195.

Torrance C., Compo GP. 1998. A practical guide to wavelet analysis. *Bulletin of American Meteorological Society* **79**, 61-78.

Tyson P, Preston-Whyte R. 2000. *The Weather and Climate of Southern Africa* (2nd edition). Cape Town, 334 pp.

Vinayachandran PN, Lizuka S, Yamagata T. 2002. Indian Ocean dipole mode events in an ocean general circulation model. *Deep Sea Research,* Part II, **49**: 1573–1596.

Webster PJ, Moore AM, Loschnig JP, Leben RR. 1999. Coupled ocean-atmosphere dynamics in the Indian ocean during 1997-98. *Nature* **401**: 356-360.

White D, Richman H, Yarnal B. 1991. Climate regionalization and rotation of principal components. *International Journal of* Climatology **11**:1–25.

Wilks, DS., 2006. Statistical Methods in the Atmospheric Sciences, 2nd Edition. *International Geophysics Series, Vol. **59**,* Academic Press, 627 pp.

Willmott, C J, Matsuura, K.1995: Smart interpolation of annually averaged air temperature in the United States. *Journal of Applied Meteorology,* **34:** 2557–586.

WMO, 1996. Climate Change, WMO technical Note No **79**. WMO No. 195-TP-100, World Meteorological Organization, Geneva, 53 pp.

Wu R, Kirtman P. 2005. Roles of the Indian and Pacific Ocean air-sea coupling in tropical atmospheric variability. *Climate Dynamics* **25**: 155-170.

Xie P, Arkin PA. 1996. Analysis of global monthly precipitation using rain gauge observations, satellites estimates and numerical model predictions. *Journal of Climate* **9**: 840 - 858.

Yamagata T, Behera1 S, Luo1 J, Masson S, Delecluse P, Gualdi P, Navarra A. 2003. Impact of the Indian Ocean Dipole on the East African Short Rains: A CGCM Study *CLIVAR. Exchanges* **27:** 43-45.

Yamagata T, Behera SK, Rao SA, Guan Z, Ashok K, Saji HN. 2004. Coupled ocean Atmosphere variability in the tropical Indian Ocean. Earth Climate: The Ocean Atmosphere Interaction, *Geophysical Monograph* **147**: 189-212.

APPENDIX A

CRAMERS' t-TEST

The formula for Cramer's t-statistic is given by:

$$t_k = \left[\frac{n(N-2)}{N - n(1+l_k^2)} \right]^{(1/2)/k}$$

Where $l_k = \frac{\left(\overline{x_k} - \overline{x}\right)}{\delta}$

And the standard deviation is given by $\delta = \left[\frac{\sum_{i=1}^{N} x_i^2}{N} - x^{-2} \right]^{1/2}$

The mean for the sub periods *k* and *n* values is $\overline{x_k} = \frac{\sum_{i=k+1}^{k+n} x_i}{n}$

And the mean for the entire record is $\overline{x} = \frac{\sum_{i=1}^{N} x_i}{N}$

The t-statistic t_k, is distributed as Student's t with (N-2) degrees of freedom, and can therefore be tested for significance (**WMO**, 1996).

APPENDIX B

PARTIAL CORRELATION ANALSIS

The partial correlation is defined as the correlation between two signals out of three or more, after the contributions from the rest of the signals have been removed.

Let r_{12}, r_{23} and r_{13} the convectional correlation between normalized time series X_1 and X_2, X_2 and X_3, and X_1 and X_3 respectively. By X_3 and X_1 onto X_2 respectively, we obtain: $X_1 = X_1^{'} + r_{12}X_2$, $X_3 = X_3^{'} + r_{23}X_2$

Here X_2 is defined as the second predictor while X_3 is predicted by the predictor X_1 after the influences of X_2 have been removed. The partial correlation $r_{31,2}$ between X_3 and X_1 is defined as the correlation coefficient between $X_1^{'}$ and $X_3^{'}$. We find $r_{31,2} = \left(r_{13} - r_{12}r_{23}\right) \Big/ \sqrt{\left(1-r_{23}^2\right)\left(1-r_{12}^2\right)}$

Similarly, we find $r_{32,1}$ as the partial correlation coefficient between X_3 and X_2. It is written as : $r_{32,1} = \left(r_{23} - r_{12}r_{13}\right) \Big/ \sqrt{\left(1-r_{13}^2\right)\left(1-r_{12}^2\right)}$

The quantity X_3 can be predicted by the predictors X_1 and X_2 by using the multi regression method. The regression equation is written as:

$X_3 = C + \delta X_1 + \varepsilon X_2$, Where C is the remainder, $\delta = r_{31,2}\sqrt{\left(1-r_{23}^2\right)\left(1-r_{12}^2\right)}$,

and $\varepsilon = r_{32,1}\sqrt{\left(1-r_{13}^2\right)\left(1-r_{12}^2\right)}$.

This partial correlation has been used to estimate the different influences of the IODZM and ENSO on southern SADC rainfall variability. More details of the partial correlation can be found in most of the standard statistical textbooks (e.g. Spiegel, 1988).

APPENDIX C

Data Set of Indices

Year	Niño 3.4	IODZMI	NESORI	SESORI	ESMDRI
1950	-0.92340	-0.38890	-0.36750	-0.03650	-0.33102
1951	0.72340	0.04093	1.11119	-0.08590	1.19712
1952	-0.22340	-0.69590	-1.29130	1.23537	-2.52663
1953	0.31290	0.38888	-0.21200	-0.34480	0.13276
1954	-1.07650	-0.64470	-0.74130	2.24716	-2.98850
1955	-2.11280	-0.30700	-0.76690	1.42567	-2.19261
1956	-0.96780	-0.34790	-0.54030	0.10838	-0.64865
1957	1.27830	0.40935	-0.40340	-0.23750	-0.16587
1958	0.12987	-0.67540	-0.55050	0.56545	-1.11597
1959	-0.36760	-0.61400	0.04750	-0.27800	0.32548
1960	0.31298	-1.81140	-1.46340	1.21565	-2.67909
1961	-0.56780	2.77333	2.82797	-1.06970	3.89765
1962	-0.78760	-0.16370	-0.23870	1.32123	-1.55993
1963	1.34540	1.96487	1.39961	-0.87320	2.27279
1964	-1.16760	-1.29970	-1.08790	0.76539	-1.85330
1965	1.65650	0.59355	0.37572	-1.45990	1.83561
1966	-0.34560	0.24561	-0.41390	-0.11790	-0.29603
1967	-0.53450	1.85230	2.05439	-1.74010	3.79453
1968	0.66780	-0.65500	0.05835	-0.03590	0.09425
1969	0.78760	0.68566	-0.67930	1.07083	-1.75015
1970	-0.94570	-1.06430	0.03304	-0.57270	0.60575
1971	-1.87450	-1.19730	-0.33770	0.55142	-0.88916
1972	2.45545	2.01603	0.48919	-1.61320	2.10239
1973	-1.94550	-0.45030	-0.68180	2.38081	-3.06260
1974	0.83455	-0.83920	-0.61420	1.05452	-1.66874
1975	1.75567	-1.87280	-0.61120	0.16460	-0.77577
1976	0.89876	0.50145	-1.15550	-0.62160	-0.53393
1977	0.82340	1.47365	0.53763	0.78895	-0.25133
1978	0.27665	0.19444	1.43854	0.59860	0.83994
1979	0.56670	-0.69590	0.40798	0.00170	0.40627
1980	0.43380	-0.50150	0.04582	0.60472	-0.55890
1981	-0.13320	-0.19440	-0.42950	-0.63000	0.20047
1982	2.29787	2.12860	2.00824	-1.49470	3.50297
1983	-0.95440	0.09210	-0.07270	-0.59010	0.51747
1984	-1.65470	-0.81870	0.76709	0.27800	0.48909
1985	0.24543	0.13304	0.27477	-0.50590	0.78070
1986	1.13440	1.05407	1.37098	-0.44920	1.82019

1987	1.39770	1.28944	-0.83980	1.00737	-1.84717
1988	-1.93440	-0.05120	-0.14890	-0.84620	0.69734
1989	0.27876	-0.53220	0.55238	0.53228	0.02010
1990	0.32340	-0.09210	-0.50240	-1.30040	0.79799
1991	1.47630	0.71636	0.10507	-1.62390	1.72895
1992	0.65440	-0.77780	-0.52050	-0.22350	-0.29702
1993	0.23450	-0.24560	-1.29430	0.53402	-1.82833
1994	1.29876	1.66809	-0.33360	-1.64470	1.31111
1995	-0.79860	-0.33770	-0.70570	0.28918	-0.99493
1996	-0.36540	-2.59940	-0.54270	0.15046	-0.69319
1997	2.58700	2.73239	2.85714	-1.00460	3.86170
1998	-1.32340	-2.06720	-1.07540	1.26344	-2.33888
1999	-1.44530	0.11257	-0.14000	-0.61600	0.47602